Université d'Ottawa · University of Ottawa

Naip (THE MURINE HOMOLOGUE OF NAIP) EXPRESSION DURING MOUSE EMBRYOGENESIS

A thesis submitted to the School of Graduate Studies and Research

In partial fulfillment of the requirement for the degree of Master of Science

Department of Biochemistry, Faculty of Medicine, University of Ottawa

by Jennifer Ingram-Crooks

ABSTRACT

The childhood spinal muscular atrophies (SMAs) are autosomal recessive neurodegenerative conditions characterized by degeneration of lower motor neurons classified based on the age of onset and clinical severity. Type I is the most common and severe form of SMA with clinical presentation either *in utero* or immediately after birth. The gene encoding NAIP (Neuronal Apoptosis Inhibitory Protein) has been proposed to be a modulator of the severity of SMA and is frequently deleted in type I SMA. In this study I have assessed *Naip* (murine homologue of *NAIP*) transcript levels during mouse embryogenesis. *Naip* mRNA is present in the developing brain and spinal cord of E9.5 to E14.5 mouse embryos as detected by various *in situ* hybridization techniques. It is also found in the embryonic liver, the branchial arches, the nasal epithelium and in the future digits. At E16.5 *Naip* transcripts were found in the marginal zone of the lateral ventricle, the follicles of the vibrissae, in the retina and in the intestinal villi. These results are the first report of *Naip* gene transcript levels in embryogenesis. One model of SMA pathogenesis involves motor neuron attrition in the second and possibly third trimester of gestation. Our observation of *Naip* transcripts in the spinal cord between E9.5 and E14 .5 (equivalent to the second trimester) is consistent with a role for *Naip* in modifying SMA severity.

TABLE OF CONTENTS

CHAPTER II: MATERIALS AND METHODS

CHAPTER III: RESULTS

CHAPTER IV: DISCUSSION

REFERENCES

LIST OF TABLES

LIST OF FIGURES

LIST OF ABBREVIATIONS

AP	alkaline phosphatase
Apaf-1	apoptosis protease activating factor 1
aw	abdominal wall
Bak	bcl-2 homologous antagonist/killer
BCIP	5-bromo-4-chloro-3-indolyl-phosphate
BCL-2	B-cell lymphoma 2
BIR	baculovirus iap repeat
bp	base pair
BSA	bovine serum albumin
^{0}C	degrees Celsius
cc	central canal
cDNA	complementary DNA
cpm	counts per minute
CNS	central nervous system
d	diencephalon
dNTP	deoxynucleotide triphosphate
DIG	digoxigenin
DNA	deoxyribonucleic acid
dpc	days post-coitum
drg	dorsal root ganglia
DTT	dithiothreitol

E9.5	embryonic day 9.5
EDTA	ethylenediamenetetraacetic acid disodium salt
4thv	fourth ventricle
fd	future digit
fl	forelimb
h	heart
hl	hindlimb
I	intestine
IAP	inhibitor of apoptosis protein
int	intercostal
kb	kilobase
kDa	kilo Daltons
lat	lateral ventricle
lb	limb
li	liver
LiCl	lithium chloride
ls	lens
m	muscle
M	molar
mba	mandibular branchial arch
MeOH	methanol
mes	mesencephalon
min	minute

ml	milliliter
mM	millimolar
mo	medulla oblongata
msc	mantle layer of the spinal cord
my	myelencephalon
mz	marginal zone
n	nasal epithelium
NAIP	neuronal apoptosis inhibitor protein
NBT	nitroblue tetrazolium chloride
nc	neopallial cortex
ne	neural epithelium
nl	neural lumen
nr	neural layer of the retina
np	nasal process
nt	neural tube
ntc	notochord
nte	neural tube epithelium
oc	optic chiasma
O.D	optical density
Oe	olfactory epithelium
os	optic stalk
ov	otic vesicle
p	pons

PBS	phosphate buffered saline
PBT	1X PBS with 0.1% Tween-20
PCR	polymerase chain reaction
R	Rathke's pouch
rhb	roof of the hindbrain
RNA	ribonucleic acid
RT-PCR	reverse transcriptase polymerase chain reaction
2mba	second branchial arch
S	somite
SDS	sodium dodecyl sulfate
SMA	spinal muscular atrophy
SMN	survival motor neuron
snRNP	small nuclear riboprotein
SSC	standard saline citrate buffer
3v	third ventricle
tel	telencephalon
tRNA	transfer RNA
Tris	tris (hydroxymethyl) aminomethane
µl	microliter
µg	microgram
µm	micrometer
UTR	untranslated region
UV	ultraviolet

v	vibrissae
wmb	wall of the midbrain

CHAPTER I:

INTRODUCTION

1. 1 CELL DEATH IN EMBRYONIC DEVELOPMENT

Embryonic development is still a poorly understood series of events and elucidation of the genetic controls of this process is underway. Development involves maturation of the biochemical pathways as well as formation and shaping of physiological functions of organs and tissues. Despite the progressive and constructive nature of development, a great deal of cell death is also taking place (Naruse and Keino, 1995). Cell death in normal development was first observed during frog metamorphosis and was then detected in both invertebrates and vertebrates (Jacobson *et al.*, 1997). The general conservation of the mechanisms, which control cell death, suggests that this phenomenon is a fundamental feature of animal cells. Thus cell death is now being accepted as a widespread feature of normal development. The ability of RNA and protein synthesis inhibitors to suppress this cell death demonstrates the requirement of *de novo* gene expression for activation of cell death, suggesting a programmed mechanism (Oppenheim, 1991). This naturally occurring cell death is termed apoptosis (Kerr *et al.*, 1972) and we now know that it results from the activation of a chain of metabolic events and specific genes (Nicotera *et al.*, 1999; Fadeel *et al.*, 1999). Morphologically, condensation of the chromatin, blebbing of the plasma membrane containing cytoplasmic organelles and internucleosomal DNA fragmentation are some of the characteristics of apoptosis (Wyllie *et al.*, 1980, 1984). The triggers are as varied as the effector and inhibitor pathways. The idea that cellular death is required for an organism's survival is

counterintuitive. However, this event has now been well documented and is postulated to serve many purposes. It aids in the sculpting of structures such as witnessed with the removal of interdigital tissue and it is an active process in the hollowing out of structures to create lumina, as seen in the intestine. Programmed cell death also removes vestigial structures and eliminates abnormal, nonfunctional, harmful or misplaced cells. Finally, apoptosis has an important role in controlling cell numbers in systems such as the CNS, where more than 50% of the neurons produced are eliminated by apoptosis during normal development (Oppenheim, 1991). Apoptosis during development has been extensively studied both in invertebrates and in vertebrates.

1.1.1 Cell death in the developing worm

The model organism for the study of development in invertebrates is the soil nematode, *Caenorhabditis elegans*. A pivotal point in programmed cell death studies came with the identification of *ced-3* and *ced-4* in *C. elegans*. In this invertebrate, 131 of the 1090 produced neurons always die before they can establish proper connections (Ellis *et al.*, 1991). Disabling mutations in either *ced-3* or *ced-4* inhibit this cell death, thereby underlining the requirement for the proteins encoded by both genes for cell death to occur (Yuan and Horvitz, 1992). Another gene, *ced-9*, counters the effects of *ced-3* and *ced-4*, and ablation of *ced-9* results in the death of neurons that normally do not die. This suggests that neuronal survival in *C. elegans* is dependent on permanent suppression, by CED-9, of an intrinsic program of cell death (Hengartner *et al.*, 1992). Many of these fundamental events in programmed cellular death have been conserved through evolution, as demonstrated by homologies in structures and conservation of function between genes

from the nematode and those of vertebrates. However, cell death in vertebrates involves many more mechanisms encoded by a greater number of genes, reflecting a complex and diverse control of the process of cell suicide.

1.1.2 Cell death genes in mammalian embryogenesis

The mammalian homologue to CED-3 is the cysteine protease identified as ICE (interleukin-1 beta-converting enzyme, 1) (Yuan *et al.*, 1993). Many CED-3/ICE family members have since been identified and have been linked to programmed cell death. They have been named caspases for their capacity to cleave at specific aspartic acids. Caspases mediate the final steps of apoptosis by activating pro-apoptotic enzymes (including themselves) and by inactivating enzymes and proteins required in vital cellular mechanisms (Porter *et al.*, 1997; Kumar, 1999).

Another family of genes that is critical to the control of apoptosis is the CED-9 mammalian homologue BCL-2 family (Tsujimoto and Croce, 1986; Hengartner and Horvitz, 1994). Bcl-2 has been localized to the outer membranes of the mitochondria, prevents cytochrome c release, caspase activation and cell death (Newton and Strasser, 1998). Family members of Bcl-2 such as Bcl-X_L (Boise *et al.*, 1993) inhibit cell death, whereas Bax (Oltvai *et al.*, 1993) and Bak (Chittenden *et al.*, 1995) counter the anti-apoptotic effect of Bcl-2. Bcl-2 and Bcl-X are expressed in complimentary and only partially overlapping spatio-temporal patterns in the CNS (Boise *et al.*, 1993; Krajewski *et al.*, 1994). Bcl-2 expression during murine embryogenesis is not only found in developing, proliferating neurons where it confers a critical cytoprotection, but also is expressed in the lung bud, intestinal epithelium, the kidney and the developing limb

(LeBrun *et al.*, 1993; Novack and Korsmeyer, 1994). In the human adult, BCL-2 neuronal expression in the spinal cord drops drastically in comparison to the levels seen ante and perinatally (Yachnis *et al.*, 1998). On the other hand, BCL-X_L expression has been documented in both the adult and developing brain (Sohma *et al.*, 1994). In the human, the greatest decline of motorneuron occurs between 12 and 16 weeks (Forger and Breedlove, 1987) which is also the period when BCL-2 down regulation has been documented. The exact function of these proteins during development has yet to be determined. While ablation of *bcl-2* causes a pleiotropy of abnormalities in various organs and results in death postnatally, CNS development is unaffected (Kamada *et al.*, 1995). *bcl-x* null mice die as embryos because of a surplus in cell death in various organs (Jacobson *et al.*, 1997). The absence of a role for Bcl-2 in the developing nervous system might be justified by a supplemental role by other members of the Bcl-2 family or even other anti-apoptotic proteins.

IAPs (apoptosis inhibitory proteins) are another family of genes that have been shown to inhibit apoptosis *in vitro* and *in vivo* (Liston *et al.*, 1996; Xu *et al.*, 1997; Lacasse *et al*, 1998) by direct inhibition of caspases activity (Deveraux *et al.*, 1997; Roy *et al.*, 1997), but their involvement in development has yet to be revealed. To date, only Survivin expression has been studied during human and mouse development. In the mouse, Survivin expression is ubiquitous early in development and becomes more restricted to apoptosis regulated tissues such as the dorsal root ganglia, hypophysis, lung, spinal cord and choroid plexus (Adida *et al.*, 1998). In the adult, *SURVIVIN* is undetectable in normal tissues (Ambrosini *et al.*, 1997). This IAP is expressed in a developmentally regulated fashion and plays a role in the balance between cell survival

and cell proliferation (Ambrosini *et al.*, 1998). The exact mechanism of action and triggers of the other IAPs remains unknown.

1.1.3 Cell death in developing nervous system

The death of cells in the developing nervous system is puzzling. It has been proposed that cell death in peripheral neurons ensure that the surviving cells match the available targets, resulting in the proper establishment of connections with trophic factor producing cells (Naruse and Keino, 1995). However, cell death prior to synapse formation has also been documented in the retina, spinal cord telencephalon and in sensory ganglia (Lance-Jones, 1982; Homma *et al.*, 1994; Blaschke *et al.*, 1996; Galli-Resta and Ensini, 1996). These observations suggest additional roles for cell death in neurogenesis.

Neuronal death in development is common, occurring in many different types of neurons (motor, autonomic, sensory) and begins very early in development and continues postnatally (Oppenheim, 1991). Cell death in distinct neuronal populations appears to be confined to a defined period that may differ between populations (Cowan *et al.*, 1984). In the rat cortex for example, there is no cell death seen at E10, most is seen after 12 days of embryonic age (E12), with a peak in programmed cell death occurring at embryonic day 14 (E14) and little death observed post-natally (Blaschke *et al.*, 1996).

The studies of mice models lacking genes involved in cell suicide have been of paramount significance in delineating their importance in modulating the development of the CNS. For example, *Apaf-1* (the mammalian homologue of Ced–4, apoptosis protease-activating factor 1) and *Caspase-9* null mice die at embryonic day 16.5 and perinatally

respectively, exhibiting reduced apoptosis in the brain resulting in severe cranio-facial abnormalities with hyperproliferation of neuronal cells (Cecconi *et al.*, 1998; Kuida *et al.*, 1998; Yoshida *et al.*, 1998). These results show that these genes are critical for normal neuronal development. The multi-factorial control of the cell suicide events is underlined when contemplating the CNS of *Bax* deficient mice, in which the pro-apoptotic gene has been ablated, and where neuronal apoptosis was still observed (Shindler *et al.*, 1997;White *et al.*, 1998). It is now believed that the intracellular balance between pro and anti-apoptotic members of the Bcl-2 family may serve as a rheostat to regulate whether a cell lives or dies in response to a given signal (Oltvai *et al*, 1993; Oltvai and Korsmeyer, 1994; Gillardon *et al.*, 1996).

The importance of the proper genetic control of programmed cell death is demonstrated in the discovery of cell death defining genes and the numerous disorders where repression or stimulation of cell death is the underlying pathological cause. It is now apparent that dysfunction of the normal control machinery of apoptosis is likely to have serious pathological consequences such as cancer, autoimmune and neurodegenerative diseases (Reed, 1999; Hetts, 1998; Stefanis *et al.*, 1997). One such example of the disregulation of apoptosis causing abnormal loss of motor neurons possibly because of the deletion of an apoptosis inhibitory gene is spinal muscle atrophy.

1.2. SPINAL MUSCULAR ATROPHY

1.2.1 Spinal muscular atrophy: clinical features

The childhood spinal muscular atrophies (SMA) are characterized by degeneration of the anterior horn cells of the spinal cord causing symmetrical limb muscle atrophy and

weakness (Brooke, 1985). The SMAs are autosomal recessive neurodegenerative conditions classified as type I (Werdnig-Hoffmann), type II and type III (Kugelberg-Welander) forms, based on the age of onset and clinical severity (Dubowitz, 1995). Type I is the most common and severe form of SMA with an onset either *in utero* or immediately after birth. Infants with this acute and fatal condition are unable to sit unaided and are at risk of recurrent chest infections, with death usually occurring before the first birthday (Hausmanowa-Petrusewicz *et al.*, 1980). Type II (intermediate form) SMA and type III (mild form) SMA are more benign conditions and the type III affected children frequently walk (Hausmanowa-Petrusewicz *et al.*, 1980). The combined frequencies for all three types of SMA is one in 10000, making this disorder one of the most common pediatric autosomal recessive disorder (Crawford, 1996).

1.2.2 Spinal muscular atrophy: morphology of motor neurons and muscle

The predominant loss of anterior horn cells of the spinal cord seen in SMA is at the cervical and lumbar levels (Fidzanska and Hausmanova-Petrusewicz, 1984). Many of the remaining neurons are shrunken and angular (Chou and Fakadej, 1971). A more diffuse CNS degeneration has been proposed where neurons of the Clarke's column and dorsal root ganglia would be affected (Peress *et al.*, 1986). Towfighi *et al.*, (1985) and Devriendt *et al.*, (1996) have also documented involvement of the thalamus, mesencephallon, pallidum, brainstem and spinal ganglia of type I SMA patients. The factor or factors underlying this neuronal susceptibility have yet to be identified (Devriendt *et al.*, 1996).

Two populations of muscle fibers are present in the muscle biopsies of SMA patients: normal or hypertrophied fibers and shrunken, denervated muscle fibers (Fidzianska *et al.*, 1984; Fidzianska *et al.*, 1990). The muscles of individuals with type I SMA have muscle fibers with reduced diameter, single distributed nuclei and small muscle cells that resemble myotubes (Hausmanowa-Petrusewicz *et al.*, 1980). These features are characteristic of fetal muscle suggesting that the failure of the muscle development was the result of a problem with the fusion rather than an atrophy of mature muscle fibers (Hausmanowa-Petrusewicz and Fidzianska, 1974; Fidzanska *et al.*, 1990). It has been thought that the lack of fusion event is followed by muscle degeneration because of a lack of innervation. A number of studies have now proposed that the opposite may also be true i.e. that the primary loss of the muscle by apoptosis causes loss of motor neurons due to target removal (Fidzianska *et al.*, 1990; Guettier-Sigrist *et al.*, 1998). The presence of immature muscle cells and motor neurons in type I SMA suggests that the death signals transpires early in development (Hausmanowa-Petrusewicz *et al.*, 1980). An interesting aspect of SMA is that the greatest decline in function occurs at the outset of the disease, suggesting a defined and limited loss of motor neurons followed by an increased stability of the surviving neurons, as opposed to a progressive loss of function over time (Crawford and Pardo, 1996). This is consistent with clinical studies of the disease, which shows a fixed, non-progressive disability (Russman *et al.*, 1992). This pattern of cell loss resembles developmental apoptosis, where loss of neurons is followed by reinforcement of the surviving neurons and hence SMA has been postulated to be a disease of apoptosis resulting from faulty genetic control (Sarnat, 1984; Oppenheim, 1991).

1.2.3 Spinal muscular atrophy: gene mapping

In 1990, types I, II and III of SMA were linked to region 5q13 of human chromosome 5 (Brzustowicz *et al.*, 1990; Gilliam *et al.*, 1990; Melki *et al.*, 1990a, 1990b). The heterogeneity of SMA is mirrored in the nature of this region that is characterized by genetic instability and DNA duplication, leading to the presence of several functional copies of various genes, as well as pseudogenes, placed in two inverted elements (Lefebvre *et al.*, 1995; Roy *et al.*, 1995; Scharf *et al.*, 1998). The search for the SMA gene culminated in 1995 with the simultaneous identification of two candidate genes: *SMN* and *NAIP*.

1.2.4 Spinal muscular atrophy: candidate genes

1.2.4.1 The SMA causative gene: SMN

1.1.4.1.1 SMN: general information

One of the SMA candidate genes, termed SMN for survival motor neuron, was cloned by Lefebvre *et al.* (1995). SMN is comprised of a telomeric *SMN1* (SMN_{tel}) and a centromeric *SMN2* (SMN_{cen}, *cBCD541*) copy that are both transcriptionally active (Lefebvre *et al.*, 1995). The two genes span 20 kb of genomic DNA and their mRNA is 1.7 kb (Lefebvre *et al.*, 1995). The centromeric and telomeric copies of the gene can be differentiated by the presence of five different nucleotides, none of which alter the protein sequence. Both copies contain nine exons and encode a 38-kDa protein but have different roles in SMA pathogenesis (Lefebvre *et al.*, 1995; Burglen *et al.*, 1996). Exon 7 of *SMN1* is deleted in 95% of SMA patients regardless of clinical severity (Lefebvre *et al.*, 1995).

Campbell *et al.* (1997) have shown that a higher number of *SMN2* copies are present in type II and III SMA patients compared to type I patients (Campbell *et al.*, 1997). Valesco *et al.* (1996) concluded that deletion of *SMN1* causes SMA of type I whereas the mutations seen in type II and III SMA are due to the conversion of *SMN1* in *SMN2* (Velasco *et al.*, 1996).

1.2.4.1.2 SMN: tissue expression

SMN is present in both tissues that are affected in SMA (motor neurons, cerebellar neurons etc...) (Steiman *et al.*, 1980; Towfighi *et al.*, 1985; Murayama *et al.*, 1991) as well as in tissues unaffected by the disease. The hippocampal and cerebellar neurons of the adult mouse brain, neurons of the medulla oblongata, pyramidal cells of the cortex, the Purkinje cells of the cerebellum of the human adult and the motor neurons of the adult human, monkey and rat spinal cord express the highest level of SMN transcript and protein (Lefebvre *et al.*, 1997; Battaglia, *et al.*, 1997; La Bella *et al*, 1998; Tizzano, *et al.*, 1998). Low levels but generally ubiquitous expression is observed in all other tissues examined (Lefebvre *et al.*, 1997).

1.2.4.1.3 SMN: function

SMN has no homologies to any known protein (Lefebvre *et al.*, 1995). SMN is found in nuclear gems (Gemini of coiled bodies), and interacts with SIP1 (SMN interacting protein 1) (Liu *et al.*, 1997). This SMN-SIP1 complex is directly involved in the biogenesis and trafficking of splicesomal snRNPs (small nuclear ribonucleoproteins) (Fischer *et al.*, 1997). SMN has also been shown to stimulate pre-mRNA splicing

(Pellizzoni *et al.*, 1998). This surprising role for SMN in RNA metabolism would make it appear as though a disregulation of mRNA generation is the pathogenic cause of SMA (Pellizzoni *et al.*, 1998). However SMN's role in the specific degeneration of motor neurons seen in SMA has yet to be delineated.

SMN is strongly expressed in the fetus and is essential for murine embryogenesis, as knocking out the single copy of *Smn* in the mouse results in embryonic death at the morula stage (Bergin *et al.*, 1997; DiDonato *et al.*, 1997; Schrank *et al.*, 1997; Viollet *et al.*, 1997). Studies of SMN protein expression in various human tissues during normal fetal and postnatal development have shown a general reduction of SMN levels in the postnatal period (Burlet *et al.*, 1998). This is consistent with the hypothesis that SMA is a developmental disease.

1.2.4.2 NAIP

1.2.4.2.1 NAIP: general information

The second SMA candidate gene *NAIP* (neuronal apoptosis inhibitory protein) was cloned in 1995 and is found on human chromosome 5q13 (Roy *et al.*, 1995). The NAIP gene contains 17 exons comprising 6.1 kb of mRNA and spans about 50 kb of genomic DNA (Roy *et al.*, 1995; Chen *et al.*, 1998). The 5' UTR spans the first 3 exons and part of the 4^{th} while exons 4 to 17 code for the protein (Roy *et al.*, 1995; Chen *et al.*, 1998). NAIP consists of 1403 amino acids with a 156 kDa molecular weight (Roy *et al.*, 1995; Chen *et al.*, 1998). 5q13 contains a variable number of copies of deleted and truncated *NAIP* as well as an intact copy next to *SMN1* (Roy *et al.*, 1995; Barnes.,

personal communication). *NAIP* was named because it contains domains with homology to baculoviral apoptosis inhibitory proteins (IAP)(Roy *et al.*, 1995).

IAP homology in the SMA region combined with the possible role of neuronal cell death in SMA suggested that mutations in the *NAIP* locus might affect normal inhibition of motor neuron apoptosis and the loss of which may contribute to the SMA phenotype (Roy *et al.*, 1995). NAIP exon 4-5 is homozygously deleted in 68% of type I SMA and 15% of type II and III (Roy *et al.*, 1995; Burlet *et al.*, 1996; Rodrigues *et al.*, 1996). Thus SMN1 is deleted with a high frequency in all forms of SMA whereas NAIP deletion occurs most frequently in the severe forms of SMA. This observation has lead to the development of a model in which *SMN1* is the main SMA gene and *NAIP* is acting as a modifier gene (Morrison, 1996; Crawford and Pardo, 1996).

1.2.4.2.2 NAIP: tissue expression and function

Hybridization of a Northern blot containing adult tissue mRNA with NAIP cDNA detected a 7 kb band in hepatic and placental RNA (Roy *et al.*, 1995). No visible bands were seen in the CNS tissue, however reverse transcriptase PCR (RT-PCR) amplification of the *NAIP* transcript using spinal cord suggests transcriptional activity in this tissue (Roy *et al.*, 1995). Experiments with adult mouse RNA has revealed expression in brain, spinal cord, liver, lungs, kidney and spleen by RT-PCR (Roy *et al.*, 1995).

Cell lines overexpressing part of the *NAIP* transcript (exon 4-15) show resistance to apoptosis when compared to control cell lines (Liston *et al.*, 1996). *In vivo* studies on rats show reduced ischemic damage in NAIP expressing neurons of the rat hippocampus (Xu *et al.*, 1997a). An extensive immunohistochemical study of the distribution of NAIP

in rat CNS has documented NAIP expression in the CNS in structures affected by SMA (motor neurons, thalamic neurons) (Xu *et al.*, 1997b). NAIP is also been shown to be an inhibitor of Caspase-3 and Caspase-7 (J. Maier, personal communication). NAIP's cellular distribution as well as its anti-apoptotic function suggests a role for NAIP in the prevention of the apoptosis of CNS cells. The loss of NAIP, an apoptotic inhibitor, in infants with the most severe form of SMA is in accordance with the pathological loss of motor neurons by apoptosis seen in SMA patients.

1.2.4.2.3 NAIP: *Naip* the murine homologue of *NAIP*

Naip, the murine homologue of *NAIP*, is localized on mouse chromosome 13 (D1-D3). This region is syntenic to the human chromosome 5 q11-q23 region harboring *NAIP* (Scharf *et al.*, 1996). *Naip* also contains three BIR domains and an ATP/GTP binding site as recognized in its human counterpart. Six copies of *Naip (Naip1- Naip6)* have been identified; however only three of these loci have the required 5' UTR to be translationally active in the CNS (Yaraghi *et al.*, 1998). An adult mouse mRNA tissue Northern blot revealed low expression levels of *Naip* mostly in the lung, spleen, liver and heart. No expression was seen in skeletal muscle (Yaraghi *et al.*, 1998). *Naip1* is expressed in the CNS while *Naip2* is expressed in the spleen (Yaraghi, *et al.*, 1999). *Naip2* differs from *Naip1* in that it contains an additional exon (exon 9a), which does not interrupt the open reading frame and shows no homology to any known motifs. Furthermore, multiple 5'UTRs have been found for *Naip2* whereas *Naip1* only has one (Yaraghi, *et al.*, 1999). The purpose of these alternatively spliced 5'UTRs has not yet been established but suggests differences in the regulation of translation of these genes (Yaraghi, *et al.*, 1999).

1.2.4.3 H4F5

Recently a third potential SMA modifying gene, termed *4F5,* has been identified (Scharf *et al.*, 1998). Human *4F5* has 5 exons and exists in two copies, both of which generate 1.8 kb and 0.7 kb transcripts. *H4F5* shows homology to a protein known to co-localize with snRNPs, which suggests a role in the same pathway as SMN. 90% of type I SMA patients are deleted for the *H4F5* copy adjacent to *SMN1* identified (Scharf *et al.*, 1998). More study into the roles of both copies will help elucidate the role of 4F5, if any, in the pathology of SMA (Gendron and MacKenzie, 1999).

1.3 THESIS OBJECTIVE AND OUTLINE

NAIP deletions occur most frequently in the severe forms of SMA (type I) which has a onset ranging from *in utero* up to six months of age. This suggests that the involvement of *NAIP* in SMA pathogenesis may occur during development. Furthermore, *NAIP* expression in adult human and mouse tissue is low, as seen by RT-PCR and Northern blots (Roy *et al.*, 1995; Yaraghi and MacKenzie, 1998). This information suggests that there may be developmental regulation of *Naip.* To explore this possibility the analysis of the spatial and temporal expression patterns of *Naip* during murine embryogenesis has been undertaken using whole mount *in situ* hybridization and ^{33}P *in situ* hybridization. *Naip* was present in the developing spinal cord, brain and liver from E9.5 to E14.5. At E16.5 *Naip* transcripts were found only in the forebrain, retina and in the villi of the intestine. While our data do not determine whether SMA is exacerbated

from impaired *NAIP* expression in the spinal cord and skeletal muscle, they are consistent with a role for *NAIP* during embryonic development.

2. MATERIALS AND METHODS

2.1 Embryos

Female CD-1 mice at Days 9.5, 10.5, 11.5, 12.5, 13.5, 14.5, 15.5 and 16.5 of timed pregnancy (where noon of the day the vaginal plug is found is designated 0.5 dpc (days post-coitum)) were received from Charles River. The uteri were collected and placed in cold PBS, and the embryos were dissected free of extra-embryonic membranes in cold PBS to prevent proteolysis. Embryos were then either frozen at -80°C (for RNA extraction), fixed for several days in formalin (for sectioning) or fixed in paraformaldehyde overnight at 4°C (for whole mount *in situ* hybridization).

2.2 Reverse Transcription and PCR of embryonic mouse RNA

2.2.1 Isolation of total RNA

Total RNA was extracted from frozen whole embryos at different developmental stages and from various adult tissues using a modified guanidine thiocynate RNA isolation kit from Clontech (ATLAS Pure RNA Isolation Kit). In brief, 100 mg of frozen tissue was homogenized with a PT 1200C polytron (Kinematica) for 1 minute on ice in 1 ml of Denaturing solution (2.7 M guanidine thiocyanate, 1.3 M ammonium thiocynate, 0.1 M NaOAc (pH 4.0)). After a 10 minute incubation on ice, samples were vortexed and centrifuged at 15,000 x g for 5 minutes at 4°C in a J2-MC centrifuge (Beckman). The supernatants were transferred to new tubes and 2 ml of buffered phenol was added. Samples were vortexed for 1 minute and then placed on ice for 5 minutes prior to the addition of 0.6 ml of chloroform. The samples were vortexed for 2 minutes and iced for 5 minutes. The homogenates were centrifuged at 15,000 x g for 10 minutes at 4°C. The

upper aqueous phase was transferred to a fresh tube where the phenol-chloroform step was repeated with only 1.6 ml of phenol. After the centrifugation step and the transfer of the upper phase to a fresh tube, 2 ml of isopropanol were added slowly with occasional mixing. The solution was placed on ice for 10 minutes and then centrifuged at 15,000 x g for 10 minutes at 4°C. The RNA pellet was washed with 80% ethanol and allowed to air dry after the ethanol was discarded. The pellets were resuspended in 100 µl of RNase-free water and DNase treated with 10 units of DNase I (Clontech) at 37°C for one hour. An equal volume of phenol:chloroform:isoamyl alcohol (25:24:1) was added to the mixture. The samples were vortexed and spun in a 5415C microcentrifuge (Eppendorf) at 10,000 rpm for 10 minutes. This step was repeated and then followed by a chloroform treatment under the same conditions. 1/10 of the volume of 2M Sodium Acetate pH 4.5 and 2.5 volumes of 96% ethanol were added to the sample. After being vortexed the samples were centrifuged for 20 minutes. The supernatant was carefully removed and the pellets were washed with 80% ethanol, spun for 10 minutes and then allowed to air dry. The pellets were resuspended in 30 µl of water and the concentration was adjusted to 1µg/µl after determining the concentration by O.D. The RNA samples were analyzed for the expression of *Naip* by RT-PCR using primers for different copies of *Naip*.

2.2.2 Reverse Transcription

The RNA was reversed transcribed and PCR amplified to ascertain the presence of the mRNA of interest. Five micrograms of total RNA isolated from adult mouse spleen and brain and from mouse embryos at different stages of development, (i.e. embryos at E10.5, E11.5, E12.5, E13.5, E14.5, E15.5 and E16.5) were reversed transcribed and the desired sequences were amplified. The templates used in PCR were generated by reverse

transcription of total RNA in the following conditions: the RNA was incubated with 0.05 μg of a specific primer and water for a total volume of 7.5 μl at 85°C for 5 minutes and then cooled on ice for an additional 5 minutes. Reverse transcription was primed off with an exon 10 primer conserved in all *Naip* copies (primer A) as well as an β-actin reverse primer that was used as a control. All *Naip* specific primers were obtained from Dr. Z. Yaraghi. The β-actin primers were designed according to Silva *et al.* (1996). Table 1 lists the *Naip* primer sequences and Figure 1 shows the relative positions of all *Naip* primers used. Table 2 lists the β-actin primers used. The 20 μl reaction consisted of the RNA/primer mixture as well as 1st strand buffer (5X) (250 mM Tris-HCl pH 8.3, 375 mM KCl, 15 mM $MgCl_2$)(Gibco), 0.01 M DTT, 2 mM dNTPs, 5 units Ribonuclease inhibitor (Gibco) and 400 units of SuperScript II Reverse Transcriptase (Gibco). After 60 minutes at 37°C the reaction was terminated by heating it to 65°C for 10 minutes.

2.2.3 Polymerase Chain Reaction amplification of RT products

A first round of PCR amplification was performed in a Perkin-Elmer Cetus DNA Thermal Cycler 480. For the first round of thirty cycles, a *Naip* exon 10 reverse primer (primer B) and a *Naip* exon 1 forward primer (primer B') were used (Table 1). Both primers recognize all *Naip* copies. The β-actin forward and reverse primers are compiled in Table 2. The 25 μl reaction contained: 5 μl of cDNA mixture, 1 unit of *Taq* DNA polymerase (Gibco), 0.4 mM of each dNTP, 1X of 10 X PCR buffer (200 mM Tris-HCl (pH 8.4), 500 mM KCl, 25 mM $MgCl_2$ (Roche)) and 0.05 μg of each primer as indicated. The following program was used: 5 minutes at 94°C, then 30 cycles of denaturing for 1 min at 94°C, annealing for 1 min at 58°C and extension for 1 min at 72°C. An additional

Primer Name	*Naip* Exon	Strand	Sequence
A	10	reverse	5' AGCGATCAATAAGCAGGTCCG 3'
B	10	reverse	5' GCAGCATCCTGATGCCCAGAG 3'
B'	1	forward	5' CTCGTGCCTGTCACCCTG 3'
C	9a	reverse	5' GAAGATAGGTCCCACTGGATG 3'
C'	9a	forward	5' TTTCTCCAAGTGAAGCCCA 3'
D	7	reverse	5' TTGTTGTGCTCTTGTATTGGG 3'
D'	2	forward	5' GGGACATCACCACGTGTACTC 3'
E'	1	forward	5' GAAGCAGGAGCCTGACTGAAC 3'

Table 1: Exon location, sequence and strand location of *Naip* specific primers used in the reverse transcription and polymerase chain reaction of total RNA from mouse embryos and from adult mouse tissues.

Figure 1: Schematic representation of the first exons of *Naip*. A) Schematic representation of the first 10 exons of consensus *Naip* depicting the relative position of primers used for the reverse transcription and PCR of total mouse embryo RNA as well as the probes used for *in situ* hybridization. B) Schematic of the first eleven exons of *Naip2*. The expected size of the amplified fragments is indicated in brackets above their relative positions in the sequence.

A)

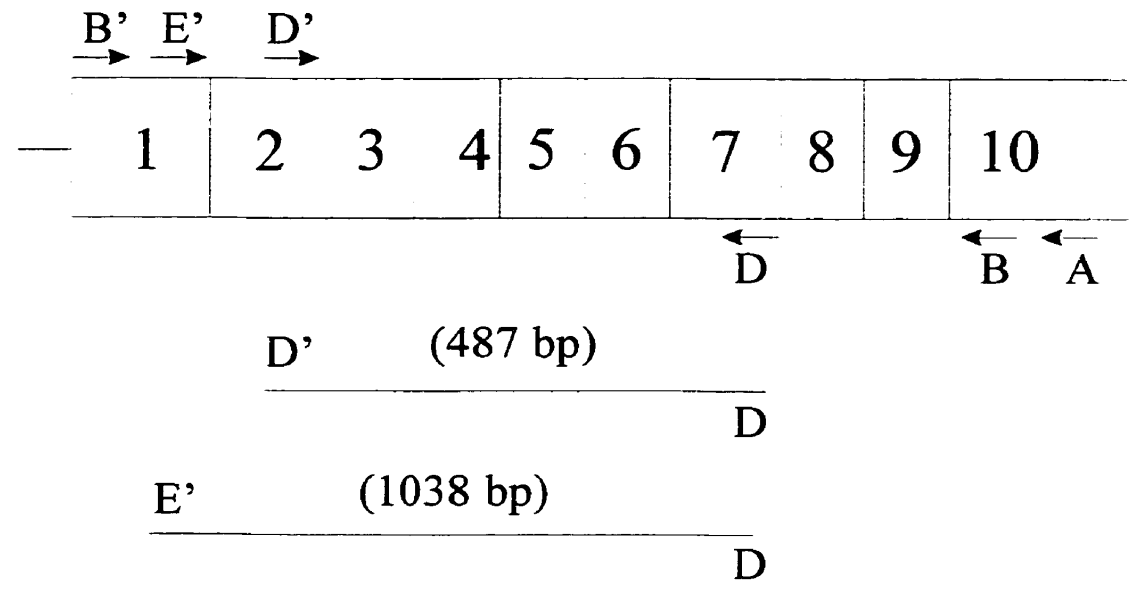
B' E' D'
1 2 3 4 5 6 7 8 9 10
D
B A
D' (487 bp)
D
E' (1038 bp)
D

B)

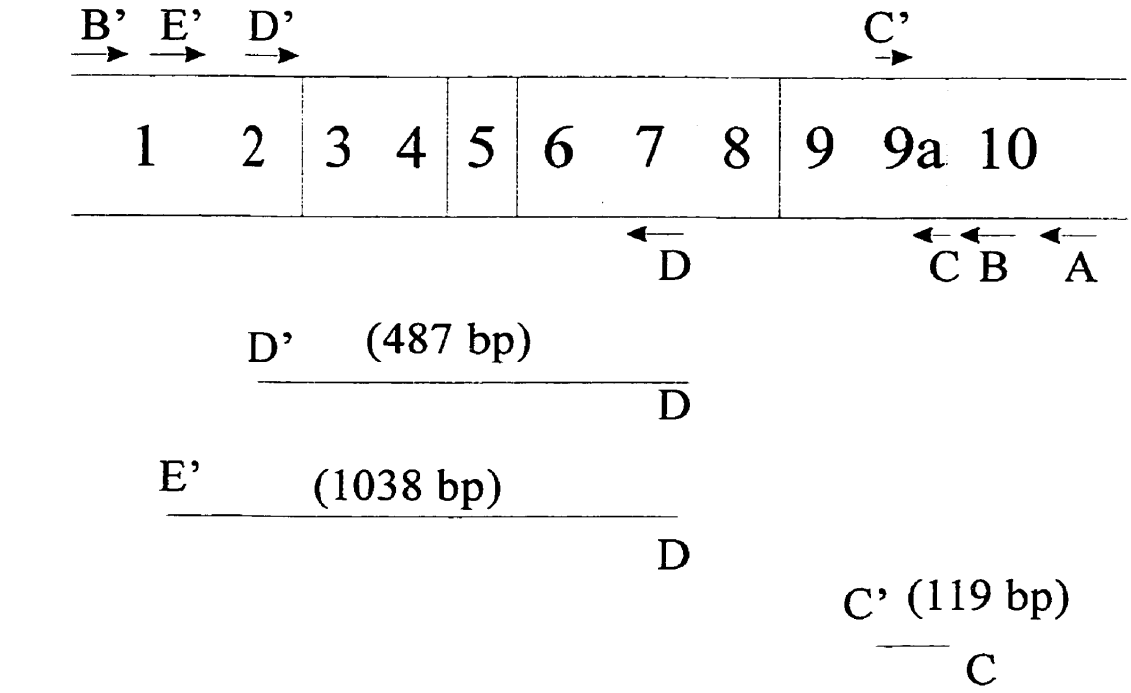
B' E' D'
C'
1 2 3 4 5 6 7 8 9 9a 10
D
C B A
D' (487 bp)
D
E' (1038 bp)
D
C' (119 bp)
C

Primer	Strand	Sequence
R-β-actin	reverse	5' AGCCATGTACGTAGCCATCC 3'
F-β-actin	forward	5' TGTGGTGGTGAAGCTGTAGC 3'
R-myogenin	reverse	5' ATAGCAACCAGTCTTTATTCA 3'
F-myogenin	forward	5' ATAGCAACCAGTCTTTATTCA 3'

Table 2: Primers used for the synthesis of β-actin and myogenin probes. β-Actin was used as a loading control in RT-PCR while myogenin was used as a positive control for *in situ* hybridization. The expected product size of β-actin is 220 bp while myogenin will yield a 415 bp product.

extension at 72°C for 10 minutes was performed and the samples were kept at 4°C thereafter.

A round of nested PCR was then performed on the amplified DNA fragments. This time 1 µl of a 1:10 dilution of the product from the first round of PCR was incubated in the same conditions as above with primers specific to various copies of *Naip* as indicated in Table 3. Twenty microliters of the nested PCR reaction was migrated on a 2% agarose gel containing ethidium bromide (0.5 µg/ml) and then photographed under UV illumination. The expected product size as well as the copy of *Naip* that is recognized by the primers used are indicated in Table 3. The sequences were verified by DNA sequencing in house (Performed by C. Neville) on a ABI 373A automated sequencer according to Applied Biosystem's instructions.

2.3 Whole Mount *in situ* hybridization

2.3.1 Synthesis of DIG labeled probes

2.3.1.1 Preparation of DIG-dNTPs

A 100 X concentrated dNTP mix was prepared as follows: 20 mM dATP, 20 mM dCTP, 20 mM dGTP and 17 mM dTTP. A 10x DIG-dNTP mix was made in a reaction volume of 50 µl as follows: 5 µl of the 100X dNTP mixture was added to 0.3 mM of DIG-11-dUTP 1mM (Digoxigenin-11-2'-deoxy-uridine-5'-triphosphate, alkali-labile (Roche)). This gives a 1:7 ratio of DIG-dUTP: dTTP.

2.3.1.2 Probe synthesis by unidirectional PCR

Naip cDNAs were provided by Dr. Zari Yaraghi and probes complimentary to *Naip* were synthesized by using unidirectional PCR. Four hundred nanograms of DNA

Primer pairs	Product size (base pairs)	Copy of *Naip* recognized
B- B'	1672	All *
C- C'	119	*Naip 2*
D- D'	487	All*
D- E'	1038	All*

Table 3: Expected product size of PCR amplified *Naip* templates using various primer pairs to different regions of the *Naip* gene. See figure 1 for relative positions of primers. Primers B/B' were used for the first round of PCR then the other primer pairs were used to perform nested PCR.

*By all, we mean *Naip1*, *Naip2* and *Naip3*; this remains unclear for *Naip4*, *Naip5* and *Naip6*

were incubated with 5 µl of 10X DIG-dNTP, 2.5 µl of 10 x PCR buffer (Roche), 1 Unit of *Taq* DNA polymerase (Gibco) and 150 ng of the reverse primer (antisense probe) or 150 ng of the forward primer (sense probe). The mixture was incubated for 35 cycles in the PCR thermal cycler under the following conditions: 94°C for 1 minute, 58°C for 1 min 30 sec, 72°C for 1 min 30 sec. Following the PCR run, the reaction was purified using QIAquick PCR purification columns (QIAGEN) according to manufacturer's instructions. Five volumes of Buffer PB were added to the PCR mix and the new mixture was placed on a QIAquick spin column to allow the DNA to bind by centrifuging the column for 30 seconds. The flow-through was discarded and the column was washed with 0.75 mL of Buffer PE (containing ethanol) and centrifuged for 30 seconds. All of the residual Buffer PE was removed by an additional 30 second spin. The columns were then placed in fresh microcentrifuge tubes and 30 µl of water was placed on the column in order to elute the sample. After allowing the columns to stand for 1 minute, they were centrifuged for 30 seconds to collect the probe. Fragment size was verified by gel electrophoresis on a 1% agarose gel containing ethidium bromide (0.5 µg/ml), and visualization was performed under UV light. While several probes were tried, only the results from the 1038 bp probe are presented. The *Naip* antisense and sense probes are 24% homologous at the nucleotide level.

2.3.1.3 Evaluation of the probe incorporation

DIG-dUTP incorporation into the single-stranded probe was evaluated using DIG quantification and DIG control test-strips as directed by the manufacturer (Boehringer Mannheim). Briefly, a series of dilutions of the DIG-labeled probe are applied to a DIG quantification strip. DIG control test-strips are already loaded with defined dilutions of a

control DNA and are used as standards. The test-strips are then subjected to immunological detection with Anti-Digoxigenin-AP (Boehringer Mannheim) and the colour substrates NBT/BCIP (Boehringer Mannheim). DIG-labeling efficiency can be determined by comparing the signal intensity of the spots on the test-strip with those of the control test-strip. Probes are used at 0.5 μg of labeled probe per milliliter of hybridization solution.

2.3.2 Preparation of embryos

In situ hybridization was performed using a modified Wilkinson protocol (Wilkinson, 1992). E9.5-E13.5 embryos were fixed overnight in 4% paraformaldehyde/ PBS-0.2% gluteraldehyde at 4^0C (PBS: phosphate buffered saline). The following day they were dehydrated by being placed twice for 10 minutes in 30%, 50%, 75%, 85%, 95% MeOH/ PBT (methanol/ PBS with Tween) and finally in 100% methanol. Embryos were then either stored in methanol at –20°C or used for whole mount *in situ* hybridization.

2.3.3 Hybridization of E9.5 to E13.5 embryos

E9.5-E11.5 embryos were left intact whereas E11.5 and older embryos were punctured in the hindbrain region with a fine needle in order to allow free exchange of reagents and probe. E12.5 and E13.5 embryos were also hemi-sectioned along the median for the same reason. All solutions and plastic-ware were RNase free and all tubes were rocked gently in a hybridization incubator to allow thorough exchange of solutions. The embryos were rehydrated at room temperature in 75% MeOH/PBT, 50% MeOH/PBT and 25% MeOH/PBT for 5 minutes in each solution. Following a 10-minute wash in PBT the embryos were bleached in 6% hydrogen peroxide for 1 hour at room temperature to

inhibit some of the endogenous phosphatase activity. They were then washed in PBT and digested in 10 μg /ml of proteinase K/PBT solution. The incubation time of the embryos in this solution was dependent on the size of the embryos and had to be optimized. E9.5 embryos were treated for 10 minutes at room temperature and for each additional day of development 5 minutes of incubation were added such that E14.5 embryos were treated for 35 minutes. Embryos were then washed in PBT and fixed in 4% paraformaldehyde/PBT-0.2% gluteraldehyde for 20 minutes at room temperature. Embryos were subsequently placed in pre-hybridization buffer (50% deionized formamide, 5X SSC pH 4.5, 1X SDS, 50 μg/ml heparin) for 1 hour at 55°C. Fifty micrograms per milliliter of yeast tRNA was added to the pre-hybridization mix and the embryos were incubated an additional hour at 55°C. Finally 0.5 μg/ml of DIG-DNA–labeled probe was added to the tRNA/pre-hybridization solution and the embryos were left overnight at 55°C.

2.3.3.1 Washing and immunological detection of hybridized embryos

Embryos were washed twice for 30 minutes at 55°C in 50% deionized formamide, 5X SSC pH 4.5 and 1% SDS (Solution 1) after which time the un-annealed probe was removed by ribonuclease treatment of the embryos. The washes involved incubating the embryos three times for 5 minutes in 0.5 M NaCl, 10 mM Tris-HCl pH 7.5, 0.1% Tween-20 (solution 2) followed by a incubation at 37°C for 30 minutes in Solution 2. The embryos were then washed twice for 30 minutes in 50% deionized formamide, 2X SSC pH 4.5 (Solution 3) at 55°C and rinsed twice in PBT for 10 minutes. The embryos were pre-blocked with 10% sheep serum, 2% BSA in PBT for 3 hours at room temperature. The sheep serum was heated to 70°C for 30 minutes prior to use in order to inactivate any

endogenous phosphatases. During this time the anti-DIG antibody was pre-absorbed (see section 2.3.3.1.1) and following pre-absorption the embryos were incubated overnight at 4°C in a antibody solution comprised of 1:2000 dilution of alkaline phospatase conjugated anti–digoxigenin antibody (Boehringer Mannheim) and 10% sheep serum, 2% BSA in PBT.

2.3.3.1.1 Preparation of the anti-DIG antibody

The mouse embryo powder was prepared as follows: E12.5 to E14.5 mouse embryos were homogenized in a minimum volume of PBS using a PT 1200C polytron (Kinematica). Four volumes of ice-cold acetone were then added. The mixture was incubated on ice for 30 minutes and then spun at 10000 rpm for 10 minutes. The pellet was washed with ice cold acetone and spun again under the same conditions. The pellet was then ground into a fine powder on a piece of filter paper, allowed to air dry and the powder was stored at 4°C.

The anti-DIG antibody was then pre-absorbed using the prepared embryo powder. For each 3 mg of embryo powder added to 0.5 ml of 10% sheep serum, 2% BSA in PBT, 1μL of anti-DIG-AP Fab antibody (Boehringer Mannheim) was added. The solution was rocked gently for at least 3 hours at 4°C and then spun down for 10 minutes at 14000 rpm at 4°C. The supernatant was diluted to 2 ml using 10 % sheep serum, 2% BSA in PBT giving a 1:2000 antibody dilution.

2.3.3.2 Post antibody washes

The embryos were washed three times for 5 minutes at room temperature in PBT before being transferred to 15 ml tubes. The PBT was changed every hour for 4 hours and the samples were then incubated overnight in PBT with gentle rocking.

2.3.3.3 Colour detection

The embryos were washed for 30 minutes in a fresh solution of NTMT (100 mM NaCl, 100 mM Tris-HCl pH 9.5, 50 mM $MgCl_2$, 0.1% Tween-20 and 2 mM levamisole). They were then placed in 0.175 mg/mL BCIP and 0.150mg/mL NBT in NTMT for 6 hours in the dark. Colour development was monitored by microscope and stopped by washing the embryos in PBT. Embryos were then photographed using a SC35 Olympus camera mounted on an Olympus SZH10 dissecting microscope.

2.3.3.4 Identification of structures

The structures were identified by correlation with those depicted in *The Atlas of Mouse Development* (Kaufman, 1994).

2.3.3.5 Controls

Various controls were used during the performance of this experiment. Along with the use of the sense probe, additional negative controls used include incubating embryos without probe or antibody, with probe and no antibody and without probe but with antibody. As a positive control *myogenin* was used as indicated in Sassoon *et al.* (1989). As a template, a 500 base pair *EcoR*1 fragment excised from the 3' end of the myogenin gene cloned into a pcDNA3 expression vector (a gift from Suzanna Drmanic). Primers were designed to amplify a 415 base pair antisense and sense probe in the same conditions as indicated above (Table 2 and section 2.3.1.2). Multiple embryos of each developmental stage were always processed concurrently.

2.4 ^{33}P Hybridization

2.4.1 Paraffin embedding and sectioning of embryos

After the embryos were removed from the uterus, they were placed in formalin for several days before being processed and embedded in paraffin. Paraffin sections were cut to 6 μm thickness, mounted on silane coated slides (Sigma) and stored at 4°C. Transverse and sagittal sections were collected.

2.4.2 Riboprobe synthesis

Two riboprobes were employed for this method. Firstly, primers containing a 5' extension corresponding to the promoter sequence of T7 RNA polymerase were synthesized. The 5' TAATACGACTCACTATAGGGAGG 3' promoter sequence was added to primers D, D', and E' (Table 1 and Table 4). The 487 base pair and 1038 base pair regions of mouse *Naip* cDNA indicated in Figure 1 were PCR amplified using one of the T7 linked primers and the corresponding "nude" primers to amplify the DNA. These templates with T7 overhangs were used in the synthesis of the riboprobes. Zero point two micrograms (0.2μg) of DNA were incubated with 0.4 mM dNTPs, 5 μl of 10X PCR buffer (Roche), 1.25 units of *Taq* DNA polymerase (Gibco) and 0.05 μg of each primer. Samples were amplified, after a ten-minute incubation at 94°C, in the following conditions: thirty cycles of 94°C for one minute, 58°C for one minute and 72°C for one minute. For synthesis of the antisense template, the T7 linked reverse primer and the corresponding "nude" primer were used, whereas for the synthesis of the sense template, the T7 linked forward primer and the corresponding "nude" reverse primer were used. Refer to Table 4 for the identification of the primer pairs used. After the PCR

Primer pairs	Product size (base pairs)	Probe
T7D- E'	1038	antisense
T7E'-D	1038	sense
T7D- D'	487	antisense
T7D'- D	487	sense

Table 4: Primer pairs used for the synthesis of templates for riboprobes used for ^{33}P- *in situ* hybridization. Primers D, D' and E' indicated in Table 1 were linked on the 5' end with the T7 RNA polymerase promoter sequence: (5' TAATACGACTCACTATAGG GAGG 3').

amplification, the reaction was purified using QIAquick PCR purification columns (QIAGEN) as indicated in section 2.3.1.2. Again the fragment size was verified by electrophoreses on a 1 % agarose gel and visualized, with the help of ethidium bromide, under UV light.

The PCR fragments with T7 overhangs were then used as templates for the synthesis of ^{33}P- radio-labeled sense and antisense RNA probes. All riboprobes were synthesized by *in vitro* transcription with a NTP mix containing ^{33}[P] UTP using a MAXIscript *In Vitro* Transcription Kit (Ambion) following the manufacturers instructions. In brief, the transcription reaction was assembled in the following order: nuclease-free water to make the total volume 20 µl, 10X transcription buffer (containing DTT), 0.5 mM ATP, 0.5 mM CTP, 0.5 mM GTP, 3.125 µM ^{33}P labeled UTP, 1 µg of the DNA template and 20 units T7 RNA polymerase. The reaction was incubated for 1 hour at 37°C. The DNA template was then removed by adding 4 units of RNase-free DNase I and incubating again at 37°C for 15 minutes. Unincorporated nucleotides were removed by size exclusion chromatography on RNase-free Sephadex G-50 spin columns (Sigma). The total amount of radioactive nucleotide incorporated in the RNA probes was quantified using a 1450 Microbeto PLUS liquid scintillation counter (WALLAC).

2.4.2.1 Control riboprobes

myogenin was used as a positive control. As the fragment was cloned in both the sense and antisense orientation, in the multiple cloning site of pCDNA3, which has the T7 promoter at the 5' end, it was not necessary to use the strategy as outlined in section 2.3.2.5. Rather the proper fragments, linearized with *EcoR1* were incubated directly in

the conditions indicated in section 2.3.2.5. The *myogenin* sense and antisense radio-labeled riboprobes were synthesized as described in section 2.4.2.

2.4.3 *In Situ* hybridization

The hybridization was carried out using a modified Wilkinson protocol (Wilkinson *et al.*, 1987). Paraffin was removed from the slide-mounted sections (prepared in section 2.4.1) with xylene, the slides were then re-hydrated in decreasing amounts of ethanol, immersed in 0.9% NaCl for 5 minutes followed by immersion in 1X PBS for 5 minutes. They were then fixed with 4% paraformaldehyde in PBS for 20 minutes and washed twice for 5 minutes in 1X PBS. Samples were digested for 5 minutes in 20 μg/ml Proteinase K (Gibco-BRL) in 50 mM Tris-HCl pH 7.2, and 5 mM EDTA pH 7.2. After washing again for 5 minutes in 1X PBS, sections were re-immersed in 4% paraformaldehyde for 20 minutes. Subsequently, slides were dipped in water and acetylated with 0.1 M triethanolamine containing 0.25% acetic anhydride in 0.9% NaCl for 10 minutes. Finally the sections were rinsed in PBS, dehydrated in increasing concentrations of ethanol, air dried and hybridized at 58°C overnight in a humidified chamber, with 40 x 10^6 cpm of each probe in 1 ml of hybridization buffer (50% formamide, 0.3M NaCl, 20 mM Tris-HCl pH 7.4, 5 mM EDTA pH 7.4, 10 mM NaH_2PO_4 pH 8.0, 1X Denhardt's, 10% Dextran sulfate).

After hybridization, coverslips were removed by incubating the sections in pre-warmed 5X SSC, 10 mM DTT at 50°C for 30 minutes. Sections were then washed at high stringency at 58°C for 30 minutes in 50% formamide, 2X SSC, 100 mM DTT. A rinse in NTE (0.5 M NaCl, 10 mM Tris-HCl pH 8.0, 5 mM EDTA pH 8.0) was followed

by a 30 minute incubation at 37°C in 20μg /ml of RNase A (Gibco) in NTE. The sections were then washed for 15 minutes at room temperature in 2X SSC and then in 0.1X SSC. After the washes the sections were dehydrated in a series of ethanol washes containing 0.3M ammonium acetate, air-dried and exposed to X-OMAT AR Kodak film for 4 days. In order to obtain cellular resolution, the sections were coated at 42°C with Kodak NTB-2 liquid autoradiographic emulsion (Inter Science) and kept in light-tight boxes with desiccant at 4°C for 25 days. Photographic development was carried out in Kodak D-19 developer for 5 minutes at 16°C. The slides were then fixed in Kodak fixer and counter-stained with a 1:100 solution of toluidine blue. The pattern observed for both the 1038 base pair and the 480 base pair anti-sense probes was identical, therefore only the results for the 1038 base pair probe are presented. Analysis was performed in light and dark field using a Zeiss microscope. As only intense signals can be visualized under bright-field conditions, a more sensitive means of visualizing the silver grains is to use dark field. Images were obtained by direct capture with a Sony PowerHAND video camera mounted on the Zeiss microscope and using Northern Eclipse software.

2.5 *In situ* hybridization of slides using a DIG riboprobe

2.5.1 Preparation of DIG labeled riboprobe

The PCR fragments with T7 overhangs synthesized in step 2.4.2 were used as the templates with the DIG RNA labeling mix 10X (Roche) to generate DIG labeled riboprobes. The DIG RNA labeling mix contains 10 mM ATP, 10 mM CTP, 10 mM GTP, 6.5 mM UTP, 3.5 mM DIG-11-UTP. Briefly, 200 ng of the PCR template was incubated with 2 μl of the 10X DIG RNA labeling mix, 2 μl of transcription buffer 10X

(400 mM Tris-HCl, pH 8.0 (20°C), 60 mM $MgCl_2$, 100 mM dithiotreitol, 20mM spermidine), 2 µl T7 RNA polymerase and water to a final volume of 20 µl. The reaction was incubated at 37°C for 2 hours after which 2 µl of RNase-free DNase I was added and incubated for another 15 minutes. The addition of 2.5 µL of 4M LiCl and 75 µl of ethanol and incubation of the reaction at –70°C for 30 minutes precipitated the RNA transcripts. Following centrifugation at 4°C at 12000 g for 15 minutes, the pellets were washed with cold 70% ethanol, centrifuged again, air dried and resuspended in RNase free water to a final concentration of 0.1 µg/µl. DIG incorporation was assessed as indicated in step 2.3.1.3.

2.5.2 *In Situ* hybridization

The slides used are prepared identically as indicated in step 2.4.1. The slides were prepared for *in situ* hybridization as indicated in section 2.4.3. The slides were prepared for hybridization as indicated in section 2.4.3 however, after rehydrating the slides in decreasing amounts of ethanol, the sections were first immersed in PBS (not NaCl) followed by a incubation in 6% H_2O_2 for 30 minutes. Also, the sections were not acetylated or dehydrated prior to hybridization. The hybridization buffer was the same as the one utilized for the whole mount *in situ* hybridization in section 2.3.3. The final concentration of the riboprobe was 0.5 µg/ml and the slides were hybridized overnight at 55°C in a humid chamber.

2.5.2.1 Washing and immunological detection of hybridized slides

The slides were washed, as were the embryos in step 2.3.3.1 except that the RNase step was omitted. The slides were treated with blocking buffer as indicated in step

2.3.3.1 and antibody binding conditions were identical to those used for the whole mounts.

2.5.2.2 Post antibody washes and colour detection

The following day, the slides were first washed three times for 5 minutes in PBT then they were washed three times for 30 minutes in the same solution. The slides were then incubated in NTMT as in indicated in step 2.3.3.3. The colour development was allowed to progress for 6 to 7 hours at 37°C. The reaction was stopped by placing the slides in PBT and then rinsing them in water.

3. RESULTS

3.1) Reverse Transcription and PCR of embryonic mouse RNA

NAIP expression was demonstrated to be very low in all adult tissues examined, with the highest expression being observed in the placenta and liver (Roy *et al.,* 1995). Murine *Naip* also exhibits low levels of expression although *Naip* is detectable by Northern analysis in the liver, lung, heart and spleen of adult mice (Yaraghi *et al.,* 1998). Given the role postulated for NAIP in a disease with antenatal onset, we were interested in assessing the distribution of *Naip* at different stages of embryonic development. Reverse transcription of total mouse embryonic RNA followed by PCR amplification was undertaken to verify the presence of *Naip* in embryonic tissue. Figure 2 shows the products of RT-PCR of mouse embryo RNA at different ages of development. The primers selected recognize *Naip 1,Naip 2* and *Naip 3* or *Naip 2* only (see tables 1 and 3). Figure 2A shows the presence of *Naip 2* in all samples examined including the adult mouse brain (lane 2). Sixty cycles of PCR amplification were required to detect the expected 119 base pair, exon 9a specific product (exon 9a is exclusively found in *Naip 2*). Figure 2B illustrates the ubiquitous presence of the expected 487 base pair product in all samples analyzed using primers D and D' which amplify all copies of *Naip* (by all, we mean *Naip 1,Naip 2* and *Naip 3*). Primers D and E' also amplify a 1038 base pair fragment from all *Naip* copies (Figure 2C). *Naip 1* specific primers failed to work (data not shown). β-actin was used as a loading control to verify that relatively equal amounts of cDNA was amplified (Figure 2D). We were unable to distinguish between the different *Naip* copies at the various developmental stages examined. *Naip* is present

Figure 2: RT-PCR of total mouse embryo RNA of different developmental stages and adult mouse spleen and brain RNA. A) Using *Naip2* specific primers (primers C and C') to perform nested PCR, cDNAs from adult mouse brain (lane 1), adult mouse spleen (lane 2), E11.5 total embryo (lane 3), E12.5 (lane 4), E13.5 (lane 5), E14.5 (lane 6), E15.5 (lane 7) and E16.5 (lane 8) were amplified after a total of 60 cycles of PCR. Lane L designates the 1 kb ladder used for the molecular weight marker. Aliquots were electrophoresed on a 2% gel to resolve the expected 119 bp fragment. B) and C) The same cDNA samples were amplified, in the same conditions, by using primer pairs D- D' and D- E' respectively. The expected fragment sizes of 487 bp and 1038 bp are indicated. D) β- Actin primers were used to amplify the same cDNAs as above. The 220 bp fragment is detectable after only 30 cycles of PCR.

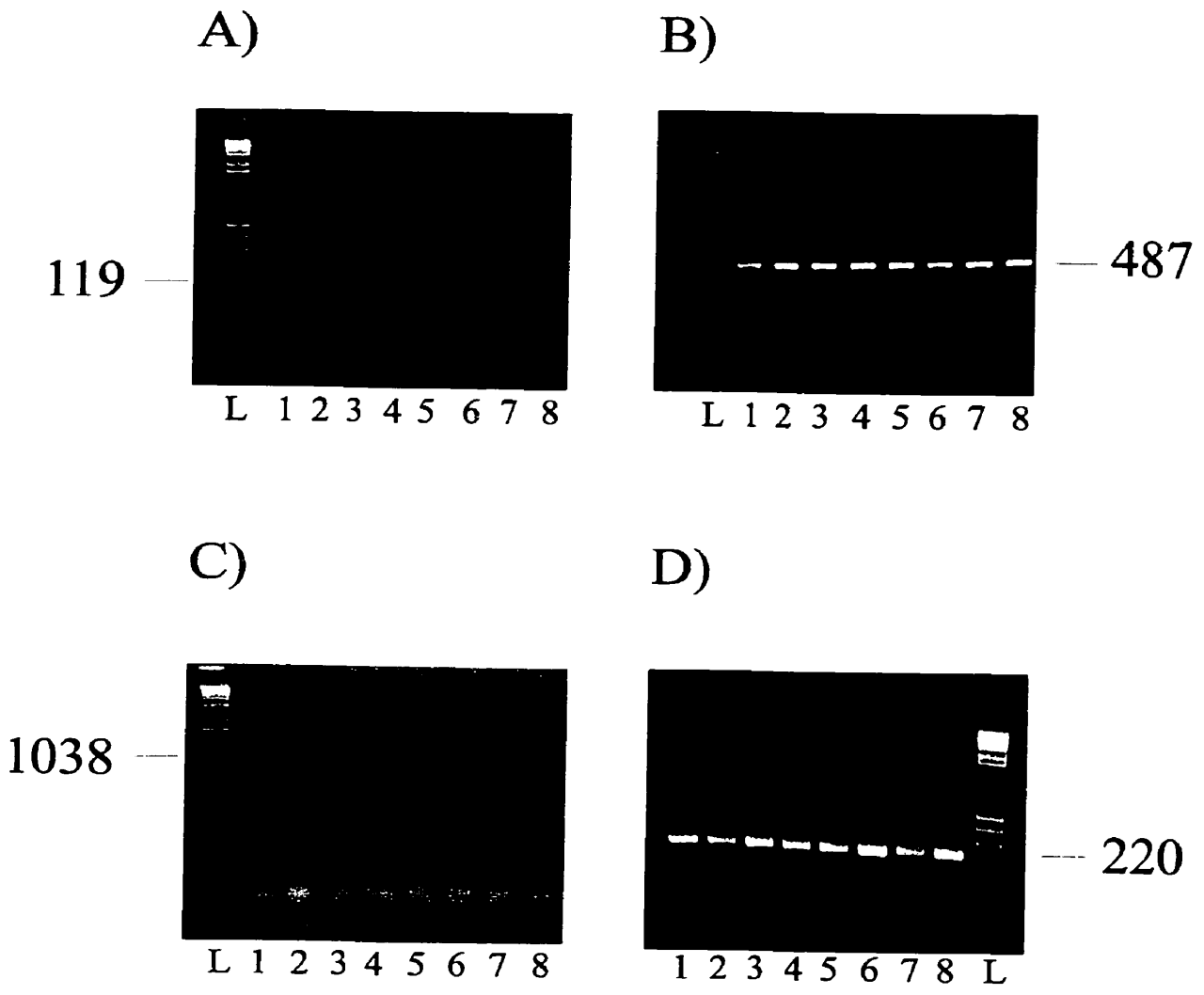
A)
B)
119
487
L 1 2 3 4 5 6 7 8
L 1 2 3 4 5 6 7 8
C)
D)
1038
220
L 1 2 3 4 5 6 7 8
1 2 3 4 5 6 7 8 L

throughout development though its transcript levels are very low, as compared to β-actin transcript levels.

3.2) Whole mount *in situ* hybridization of mouse embryos with a *Naip* specific probe

Naip expression patterns were assessed during mouse embryonic development using whole mount *in situ* hybridization. This technique allows visualization of transcripts without the necessity of sectioning the tissues. This is feasible only in embryos younger than 13.5 dpc as the higher level of organogenesis of the older embryos makes probe penetration into individual organs impossible. Nonetheless, this approach also has the advantage of permitting the simultaneous processing of several embryos which allows for a time course study to be undertaken as well as having numerous samples of a given age.

The hybridization of E9.5 to E11.5 embryos with a *Naip* antisense probe revealed staining primarily in the CNS. In E9.5 samples, *Naip* transcripts were detected in the fourth ventricle as well as in the rostral neuroepithelium of the neurotube (Figure 3A). This pattern was the same in E10 embryos with the expression in the neurotube progressing more caudally (Figure 3A) and into various brain structures. The staining in different structures of the brain becomes more prominent in E11 and E11.5 embryos (Figure 3A and 3C). The sense labeled *Naip* probe, used to assess background staining, was limited to the otic vesicle of E11.5 embryos (Figure 3B). E11.5 embryos revealed *Naip* distribution in the periphery of the telencephalic vesicle, in the mesencephalic

Figure 3: Whole mount *in situ* hybridization of E9.5 to E11.5 mouse embryos with the 1038 base pair *Naip* probe. A) *Naip* expression was detected in the fourth ventricle (4thv) and neuroepithelium (ne) of the neural tube of E9.5. E10, E11 and E11.5 embryos (x15). *Naip* is also distributed in the CNS of E11 and E11.5 mouse embryos. B) The staining of the antisense probe was compared to that of the sense probe to estimate the levels of background. The otic vesicle (ov) in E11.5 embryos is labeled with the sense probe. C) E11.5 embryos showed presence of *Naip* at the margin of the mandibular component of the first branchial arch (mba) as well as that of the second branchial arch (2ba) when compared to the sense labeled embryo (C; left-sense, right-antisense). *Naip* was also found at the periphery of the telencephalic vesicle (tel), the mesencephalic vesicle (mes) and fourth ventricle and along the neuroepithelium of the spinal cord (ne)(x15). D) *myogenin* was used as a positive control and displayed staining in the somites (S) of E10.5 and E11.5 mouse embryos (x15).

A) Antisense

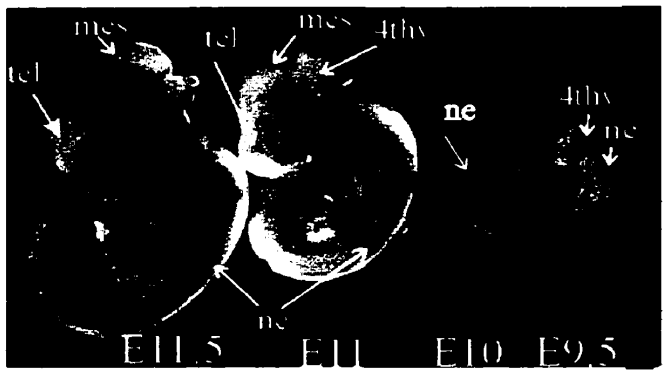

B) Sense

C) Sense Antisense

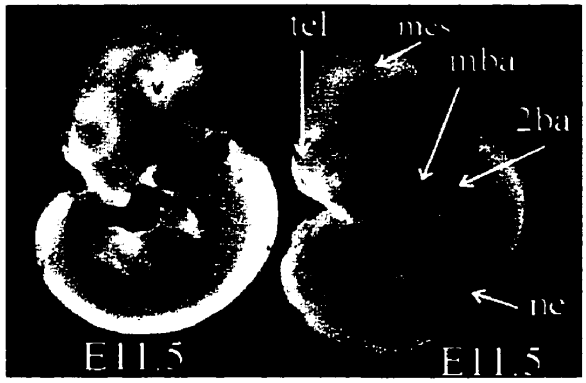

D) Antisense

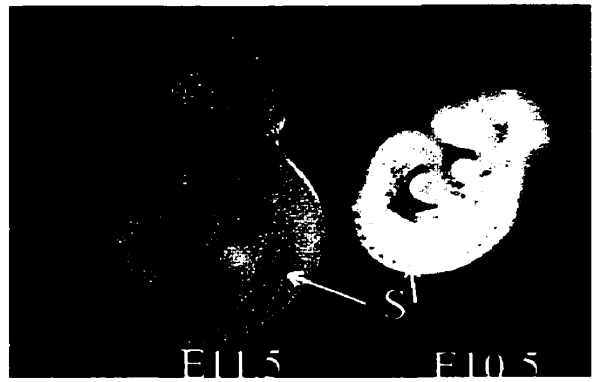

vesicle as well as in the fourth ventricle and dorsal root ganglion of the spinal cord (Figure 3C). Additional staining on the periphery of the mandibular component of the first branchial arch as well as that of the second branchial arch (Figure 3C) was observed. Comparison of the sense labeled embryos (left) with the antisense-labeled embryo (right) reveals otic vesicle staining in both precluding a determination of whether *Naip* is expressed therein (Figure3C). *myogenin* was used as another control and expression in the somites was seen as identified by Sassoon *et al.*, (1989) (Figure 3D). The use of *myogenin* as an antisense control permits a comparison with the staining pattern obtained for *Naip* and confirms a very different expression pattern for E11.5 embryos (Figure 3C and 3D). No staining was detected in the embryos incubated in the absence of probe or antibody or both (not shown). It is important to note that the level of background obtained varied from embryo to embryo regardless of the probe used even under identical situations (Figure 3C and 3D).

Older embryos (E12.5- E13.5) were hemi-sectioned along the midline to allow a better diffusion of the probe. Hybridization of E12.5 embryos brought to light *Naip* expression in the spinal cord, CNS, in the nasal epithelium and future digits of the forelimbs and hindlimbs (Figure 4A). A view of the innermost side of the section allows the visualization of specific brain CNS structures expressing *Naip*. Among these is the wall of the midbrain, the medulla oblongata as well as the wall of the neopallial cortex (Figure 4B). An examination of the dorsal region of E12.5 mouse embryos labeled with the Naip antisense (Figure 4C) and sense probes (Figure 4D) showed *Naip* transcripts to be present along the spinal cord and in the hindbrain although the exact structures that were labeled are difficult to identify in this manner. In the developing limbs, *Naip* was

Figure 4: Whole-mount *in situ* hybridization of E12.5 mouse embryos with a 1038 base pair *Naip* probe. E12.5 were hemi-sectioned along their midline prior to hybridization with the *Naip* probe. A) and B) E12.5 embryos showed *Naip* in the nasal epithelium (n), the future digits of the forelimb (fl) and hindlimb (hl), the spinal cord (sc), the wall of the midbrain (wmb), the medulla oblongata (mo) and the wall of the neopallial cortex (nc) (x10). C and D show a dorsal view of a whole E12.5 embryo labeled with *Naip* antisense and sense probes respectively (x10). E and F are close ups of the hindlimb and forelimb of E12.5 embryos showing the presence of *Naip* in the future digits (x40). G) The *Naip*-DIG-sense labeled embryos showed no specific staining nor did the *myogenin* DIG-sense labeled embryos (G and H (left))(x10). The *myogenin* antisense-labeled probe displayed staining in the somites (s), in the intercostals (int) and in other muscle anlagens (m) as previously described by Sassoon *et al.* (1989).

A) Antisense

B) Antisense

C) Antisense

D) Sense

E) Antisense

F) Antisense

G) Sense

H) Sense Antisense

identified in the future digits of the hindlimbs (Figure 4E) as well as at the dorsal surface of the forelimb (Figure 4F) and in the nasal epithelium. As with whole-mounts, antisense-labeled embryos were always compared to the staining pattern obtained with that of the *Naip* sense labeled embryos (Figure 4G) as well as that of the antisense and sense labeled *myogenin* labeled embryos (Figure 4H).

In the E13.5 mouse embryos *Naip* is still present in the nasal epithelium, the spinal cord and the wall of the midbrain (Figure 5A). Additionally *Naip* was found to be present in the myelencephalon, diencephalon, pons, tongue and the wall of the midbrain (Figure5B) when compared to the *Naip* sense labeled embryos. The dorsal view of that same section shows strong presence of *Naip* along the entire spinal cord (Figure 5C). Closer examination of the spinal cord of E13.5 mouse embryos labeled with *Naip* antisense probe presented staining in the mantle layer of the spinal cord of the lumbo-sacral region as well as in the dorsal root ganglia (Figure 5D).

3.3) *in situ* hybridization of mouse embryos sections with a ^{33}P- labeled *Naip* specific riboprobe

Radio-labeled riboprobe were used to study *Naip* gene expression in mouse embryo sections as sectioning of the whole mounts as well as use of DIG- labeled probes directly on sections failed to produce a visible signal. This method was used to confirm the results of the whole mount *in situ* hybridization experiment as well as to identify novel *Naip* containing tissues.

Figure 5: Whole-mount *in situ* hybridization E13.5 mouse embryo with a 1038 base pair *Naip* probe. E13.5 embryos were hemi-sectioned along their midline prior to hybridization with the *Naip* probe. A1) and A2) *Naip* was present in the nasal epithelium (ne), the wall of the midbrain (wmb) and the mantle layer of the spinal cord (sc) when the DIG-*Naip* antisense E13.5 mouse embryos were examined (x10). B1) An inner view revealed additional *Naip* expression in the myelencephalon (my), the diencephalon (d), the pons (p) and in the tongue when compared to the *Naip* sense labeled embryos (B2)(x10). C) A dorsal view of E13.5 *Naip* antisense-labeled mouse embryo reveals staining along the entirety of the spinal cord (x10). D) A close up of the spinal cord area revealed staining in the dorsal root ganglia (drg) (x30), inset (x15).

A)

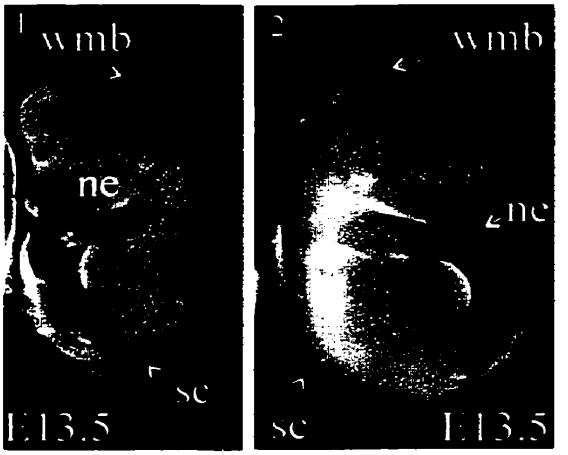
1
wmb
ne
sc
E13.5
2
wmb
ne
sc
E13.5

B)

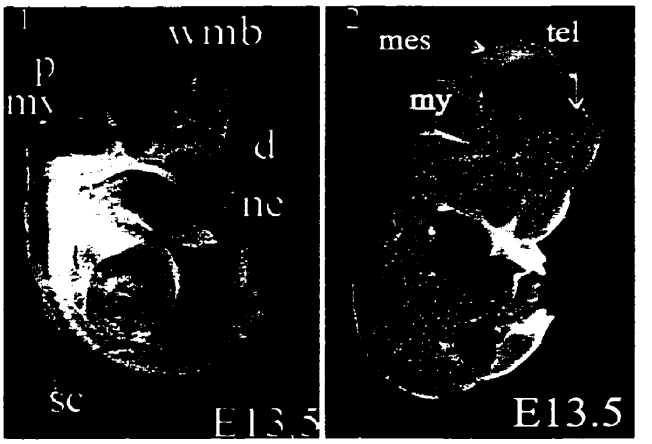
1
wmb
p
my
d
ne
sc
E13.5
2
mes
tel
my
E13.5

C)

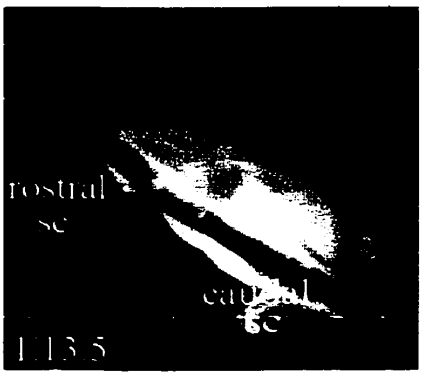
rostral
sc
caudal
sc
E13.5

D)

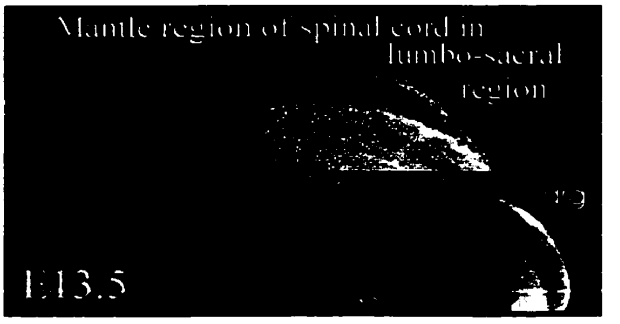
Mantle region of spinal cord in
lumbo-sacral
region
E13.5

For E9.5 mouse embryos, *Naip* expression was present in all tissues studied. *Naip* was identified in the neuroepithelial lining of the forebrain (telencephalic vesicle), midbrain (mesencephalic vesicle) and hindbrain (fourth ventricle) (Figure 6A). The presence of *Naip* was determined in comparison to the corresponding *Naip* sense labeled sections where labeling was absent (Figure 6B). Figure 6C and figure 6D show the dark field and light field micrographs of the *Naip* antisense E9.5 labeled neuroepithelium of the neural tube and the mandibular component of the first branchial arch. The neuroepithelium of the neural tube is labeled all the way to the lower extremity as seen in figure 6E and comparison to the *Naip* sense labeled section in figure 6F.

From E9.5 onwards, the *Naip* gene is expressed within certain organs of the developing embryo. E10.5 mouse embryo sections probed with a *Naip* antisense probe showed Naip expression to be similar to that seen in E9.5 mouse sections. Again the neuroepithelium surrounding the telencephalic vesicle, mesencephalic vesicle and fourth ventricle expressed *Naip* (Figure 7A). In addition, *Naip* transcripts were found in cells surrounding the optic stalk. Naip gene expression was observed again in the mandibular component of the branchial arch but was absent in the heart (Figure 7B). Figure 7C and figure 7D show *Naip* expression in the neuroepithelium of the neurotube and in the tail region respectively. None of the *Naip* sense labeled sections showed significant expression (Figure7, panels on the right).

E11.5 mouse embryo sections labeled with a *Naip* ^{33}P antisense probe also exhibited *Naip* presence at the periphery of the telencephalic vesicle, optic stalk, in the nasal process, in cells surrounding the mesencephalic vesicle, the fourth ventricle and otic vesicle (Figure 8A, B and C). Figure 8D shows *myogenin* expression the somites of

Figure 6: ^{33}P *in situ* hybridization of E9.5 sagittal mouse embryo sections with a 1038 base pair *Naip* probe. A) *Naip* expression was detected in the tissues of the telencephalic vesicle (tel), mesencephalic vesicle (mes) and fourth ventricle (4thv)(x10). B) Labeling with the corresponding sense probe did not reveal significant background. C) N*aip* was present in the tissues surrounding the neural lumen (nl) as well as in the maxillary component of the first branchial arch (mba). D and insets of A, B, E and F) Light field micrographs of the counter-stained sections. E) *Naip* was identified in the neuroepithelium of the neural tube (nte) as seen when compared to the sense labeled section in F.

A)

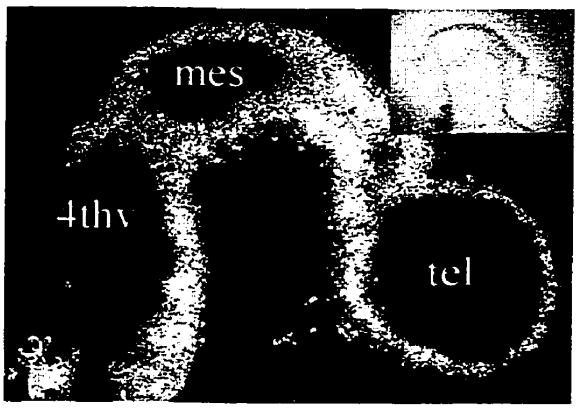

B)

C)

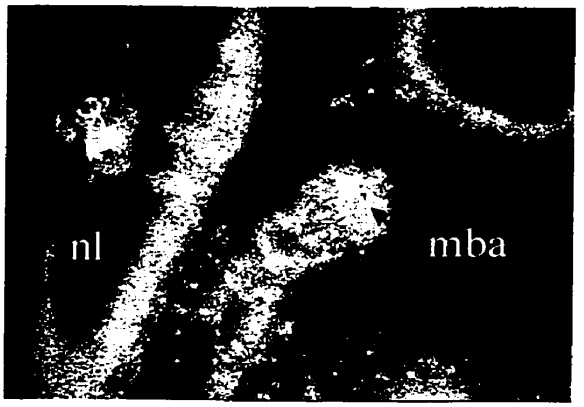

D)

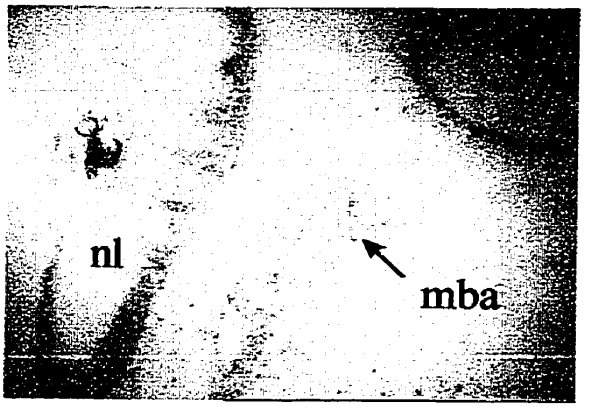

E)

F)

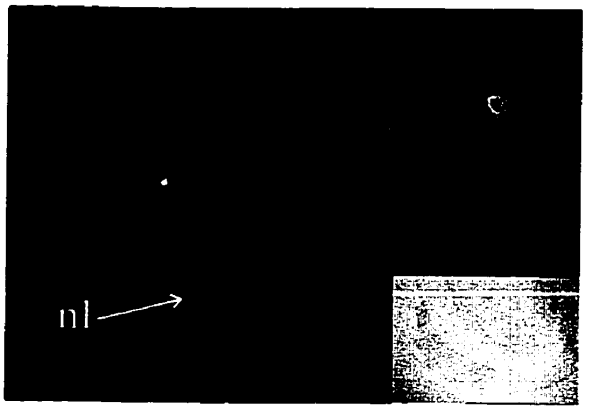

Figure 7: ^{33}P *in situ* hybridization of E10.5 sagittal mouse embryo sections with a 1038 base pair *Naip* probe. A) *Naip* expression was high in the neuroepithelial wall of the midbrain (ne) and in the tissues surrounding the telencephalic vesicles (tel), mesencepahlic vesicle (mes), the 4th ventricle (4thv), the mandibular component of the first branchial arch (mba) and the optic stalk (os). Panels on the right illustrate sense labeled sections as well as their respective light field micrograph. B) *Naip* expression was absent in the heart (h) (x10). C and D) *Naip* was identified in the neuroepithelium of the neural tube (nte) in the tail region (x10). Limb bud (lb). Silver grains present in sense labeled sections are due to background.

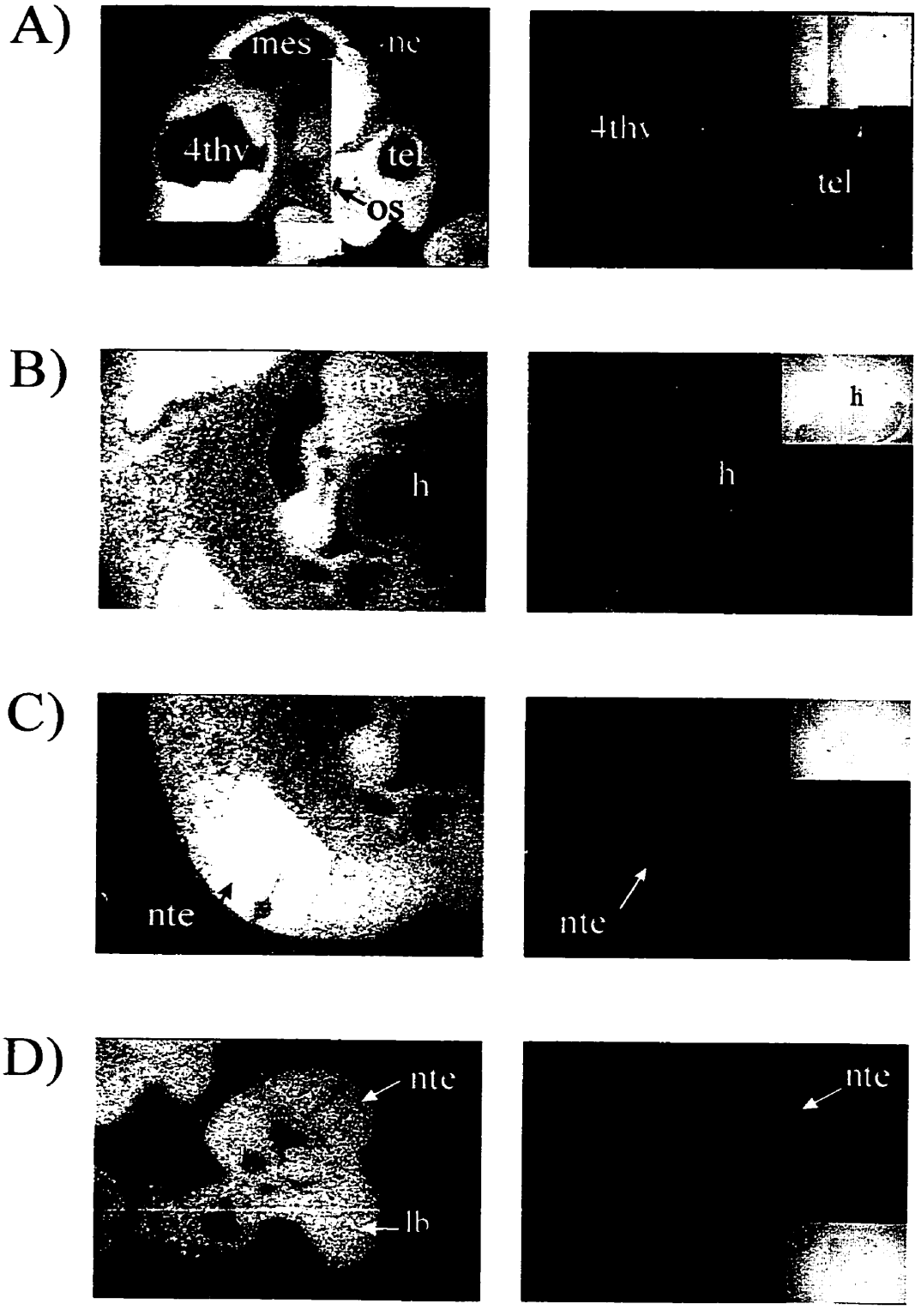
A)
mes
4thv
tel
os
4thv
tel
B)
h
h
C)
nte
nte
D)
nte
lb
nte

Figure 8: *in situ* hybridization of E11.5 sagittal mouse embryo sections with a 1038 base pair *Naip* probe. All panels are laid out such that the antisense labeled section is on the left and the sense labeled sections are on the right. A) *Naip* was detected in the nasal process (np) and at the periphery of the telencephalic vesicle (tel) as well as the optic stalk (os)(x10). B) *Naip* was also present in the mesencephalic vesicle (mes) (x10). C) Strong signal was observed in the tissue surrounding the 4^{th} ventricle (4thV) as well as the otic vesicle (os)(x10). D) E11.5 mouse embryos labeled with P^{33} *myogenin* antisense probes demonstrated its presence in the somites as described by Sassoon *et al.* (1989). E) A sagittal section demonstrating *Naip* presence in the fourth ventricle as well as in the roof of the hindbrain (rhb) (x10). F) *Naip* was also detected in the tissue surrounding the fourth ventricle when using a DIG labeled antisense probe (x20). G) *Naip* was present in the mandibular component of the first branchial arch (mba), in the hepatic primordium (hp) and absent in the heart (h) (x10). H) Again the DIG labeled *Naip* probe displayed the same pattern of expression as that seen with the ^{33}P labeled probes (x10).

A)

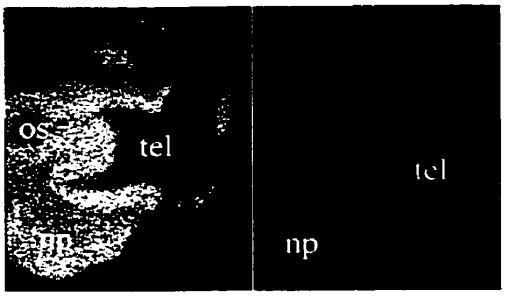
os
tel
tel
np
np

B)


mes
mes

C)

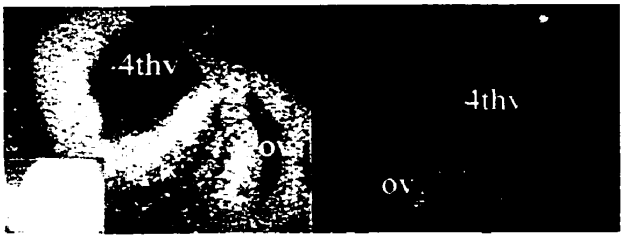
4thv
4thv
ov
ov

D)

E)


4thv
rhb
rhb
4thv

F)

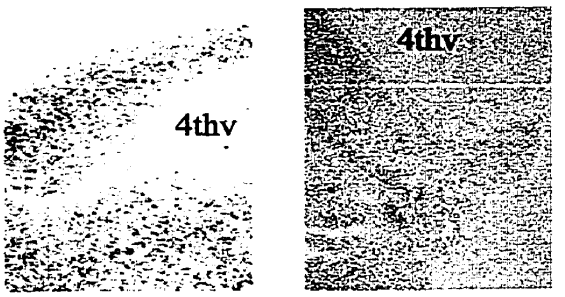
4thv
4thv

G)

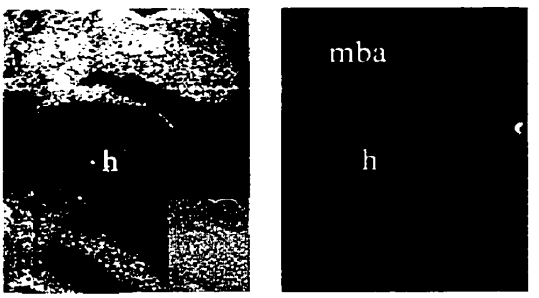
h
mba
h

H)


h

E11.5 embryos. Figure 8E is a sagittal section through the fourth ventricle showing the presence of *Naip* transcripts at the periphery of the ventricle as well as in the roof of the hindbrain. This pattern was confirmed when a DIG-*Naip* antisense probe was used (Figure 8F). *Naip* transcripts were still detectable in the mandibular component of the first branchial arch and in the liver primordia but not in the heart (Figure 8G and H). Parasagittal sections of E11.5 mouse embryo labeled with a DIG-*Naip* antisense riboprobe revealed *Naip* expression in the neuroepithelium of the neurotube (Figure 9A), as did the ^{33}P *Naip* antisense probe (Figure 9B). Sagittal sections demonstrated the presence of *Naip* transcripts in the posterior dorsal root ganglia (Figure 9C). *Naip* sense labeled sections showed little labeling (Figure 9D). Analysis of transverse sections, through the upper portion of the central canal at the level of caudal hindbrain, revealed *Naip* transcripts to be diffusely present throughout the neural tube (Figure 9E).

Figure 10 A and B demonstrate the presence of *Naip* transcripts in the lateral ventricle of E12.5 mouse embryo sections as seen in a parasagittal and sagittal section respectively. At this stage of development, *Naip* RNA was still present in the nasal epithelium (Figure 10C) and in the wall of the midbrain (Figure 10D). *Naip* was also still identified around the third ventricle and fourth ventricle in both sagittal (Figure 10 E and F) and parasagittal sections (Figure 10G). *Naip* expression continued in the liver (Figure 11A) and in the posterior dorsal root ganglion (Figure 11C). The heart still did not display the presence of *Naip* transcripts (Figure 11A) however the mantle layer of the spinal cord (Figure 11B) and the future digits of the hindlimb (Figure 11D) did.

Analysis of six-micrometer thick sections of E13.5 mouse embryos showed very faint labeling with the ^{33}P *Naip* antisense probe (Figure 12 A and B, center panels). In an

Figure 9: ^{33}P *in situ* hybridization of E11.5 mouse embryo sections with a 1038 base pair *Naip* probe with focus on the staining in the neuroepithelium. A), B) and C) *Naip* was detected in the neuroepithelium of the neural tube (ne) as well as in the posterior dorsal root ganglions (drg). A) Results from DIG-*Naip* antisense probe as compared to the sense labeled section on the right (x10). B), C) The panels on the left are the dark field of the *Naip* antisense labeled sections and the panels on the right are the respective light field exposures. D) Dark field micrograph of *Naip* sense labeled sections did not show specific staining of the neuroepithelium (ne) (x10). E) Transverse sections through the central canal (cc) revealed *Naip* to be localized in the neural tube (nt) when compared to the sense labeled sections (right panel). Inset of right panel is the light field exposure of the sense labeled section.

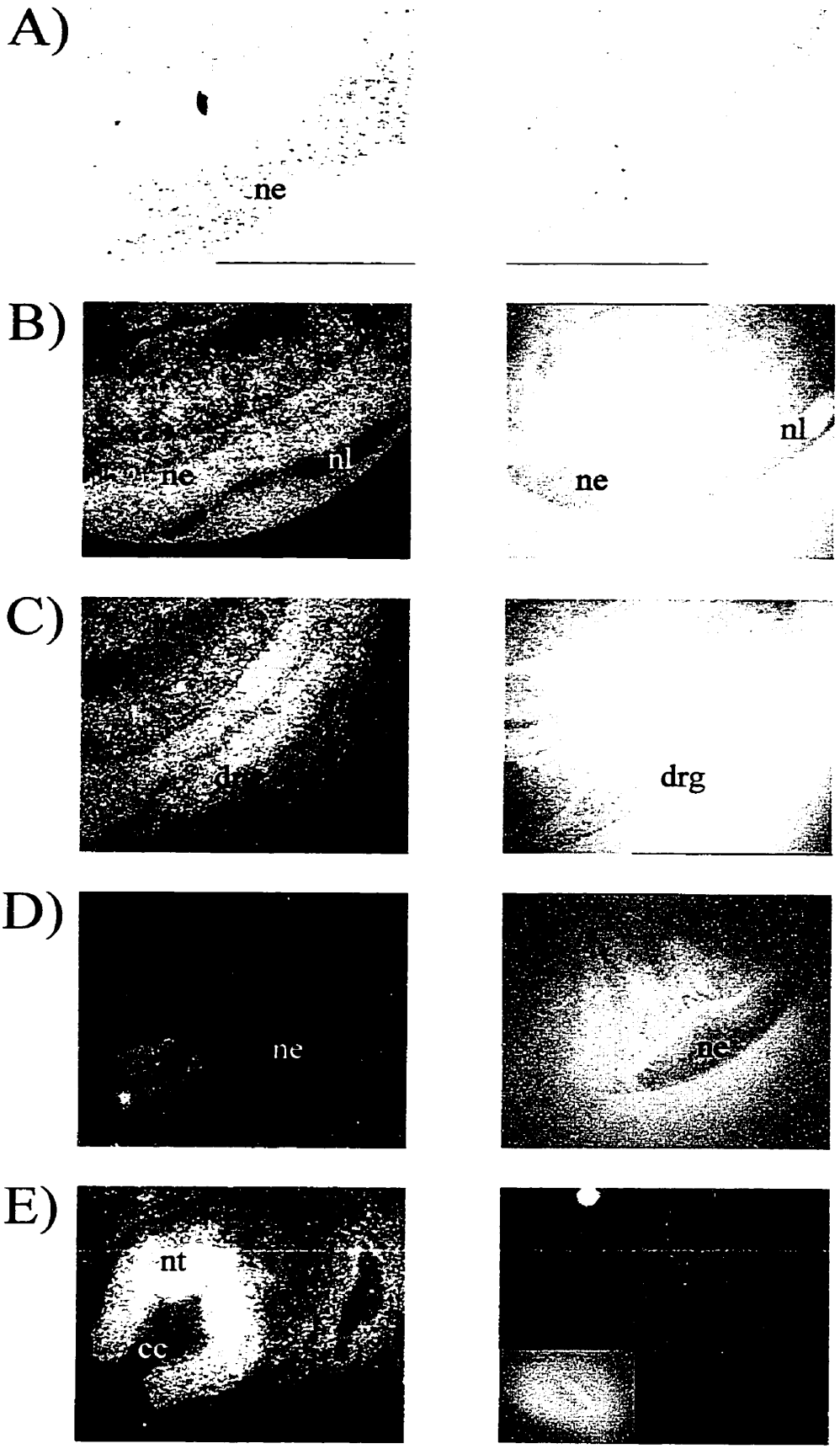
A)
ne
B)
ne
nl
nl
ne
C)
drg
D)
ne
ne
E)
nt
cc

Figure 10: ^{33}P *in situ* hybridization of E12.5 mouse embryo head sections with a 1038 base pair *Naip* probe. Left panels are antisense-labeled sections and right panels are sense labeled sections. A) and B) are parasagittal and sagittal sections respectively of the lateral (lat)ventricle. *Naip* expression was found at the periphery of the lateral ventricle as well as in the roof of the neopallial cortex (nc)(x10). C) *Naip* transcripts were also detected in the nasal epithelium of sagittal sections (n). D) The walls of the midbrain (wmb) as well as the caudal mesencepahlic vesicle (mes) were found to be *Naip* positive (x10). E) and F) are sagittal sections showing the presence of *Naip* in the third ventricle (3v) as well as in the fourth ventricle (4thv)(x10). G) The labeling of the fourth ventricle continues through to parasagittal sections (x10). H) *Myogenin* antisense labeled sections demonstrated its presence in the somites (x10).

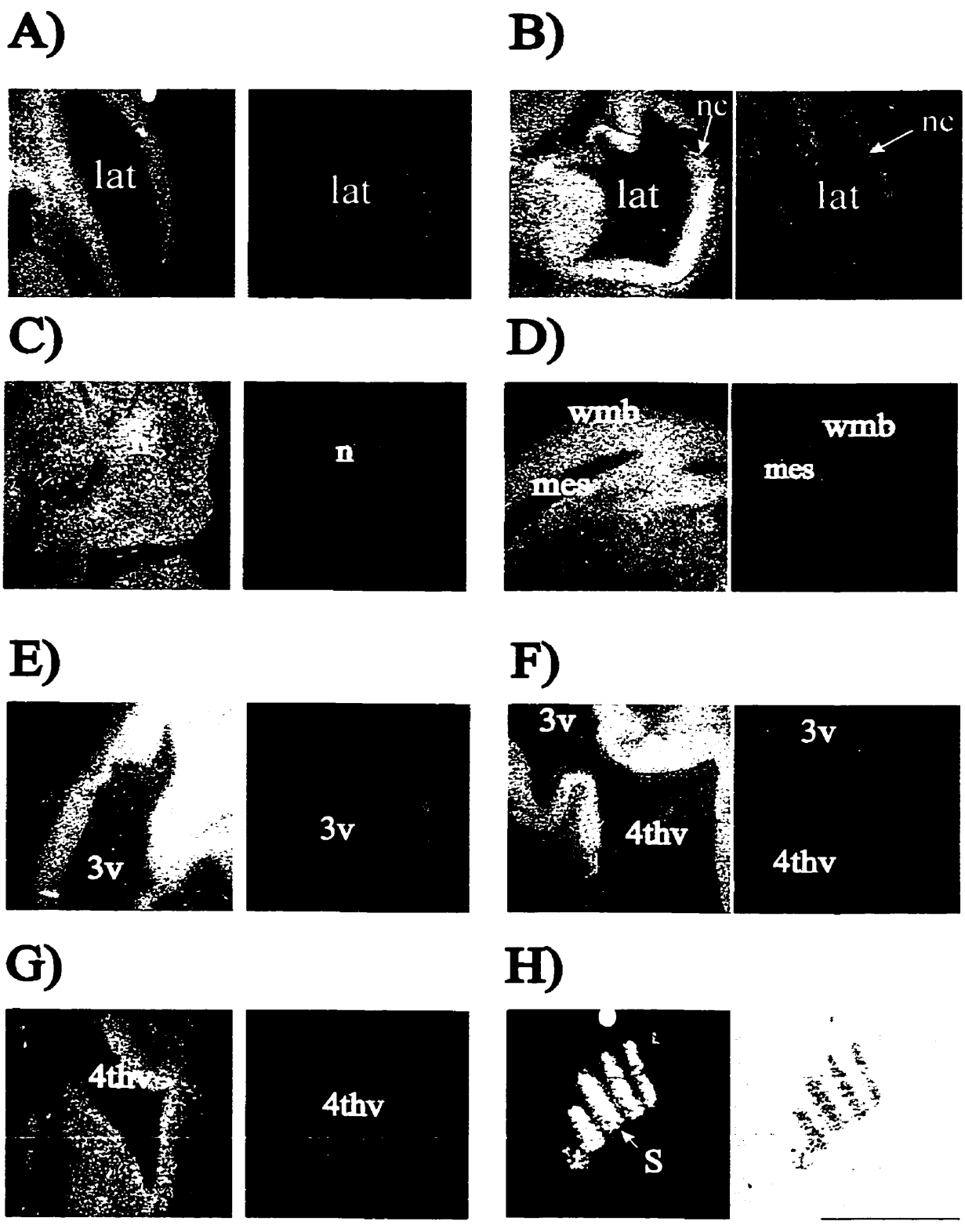
A)
lat
lat
B)
nc
lat
nc
lat
C)
n
D)
wmb
mes
wmb
mes
E)
3v
3v
F)
3v
4thv
3v
4thv
G)
4thv
4thv
H)
S

Figure 11: ^{33}P *in situ* hybridization of E12.5 mouse embryo sagittal sections with a 1038 base pair *Naip* probe. Left panels are antisense-labeled sections and right panels are the sense labeled counterparts. A) *Naip* was distributed in the liver (li) and not the heart (h) of E12.5 mouse embryo sections (x10). B) and C) The mantle layer of the spinal cord (msc) as well as the dorsal root ganglia (drg) were positive for the presence of *Naip* (x10). D) The future digits of the hindlimb also showed the presence of *Naip*.

A)

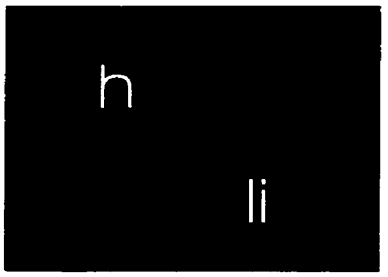

B)

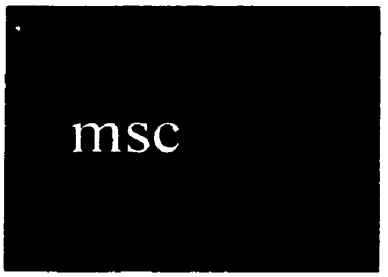

C)

D)

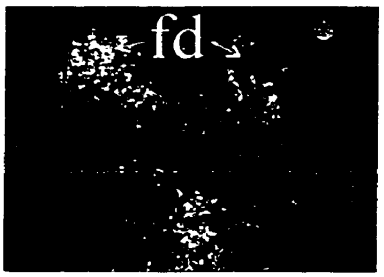

Figure 12: *in situ* hybridization of E13.5 mouse embryo sagittal sections with a 1038 base pair *Naip* probe. Panels on the left are dark field micrographs of ^{33}P *Naip* antisense-labeled 16 μm sections with their respective light field exposure inset. Panels on the far right are dark field exposures of 6 μm thick sections labeled with a ^{33}P Naip sense probe. Panels in the center are either 6 μm thick sections labeled with a ^{33}P *Naip* antisense probe (A and B) or 6 μm thick sections labeled with a DIG-*Naip* antisense probe (C, D, and E). All insets are the respective light field exposures of the sections. A) *Naip* was found in the surrounding tissue of the fourth ventricle (4thv) as well as in the nasal epithelium (n) (B), in the wall of the midbrain (wmb), in the neighboring of the mesencepahlic vesicle (mes) (C) and in the striatum (st) (D) (x10). E) *Naip* was present in the mantle layer of the spinal cord (msc)(x10).

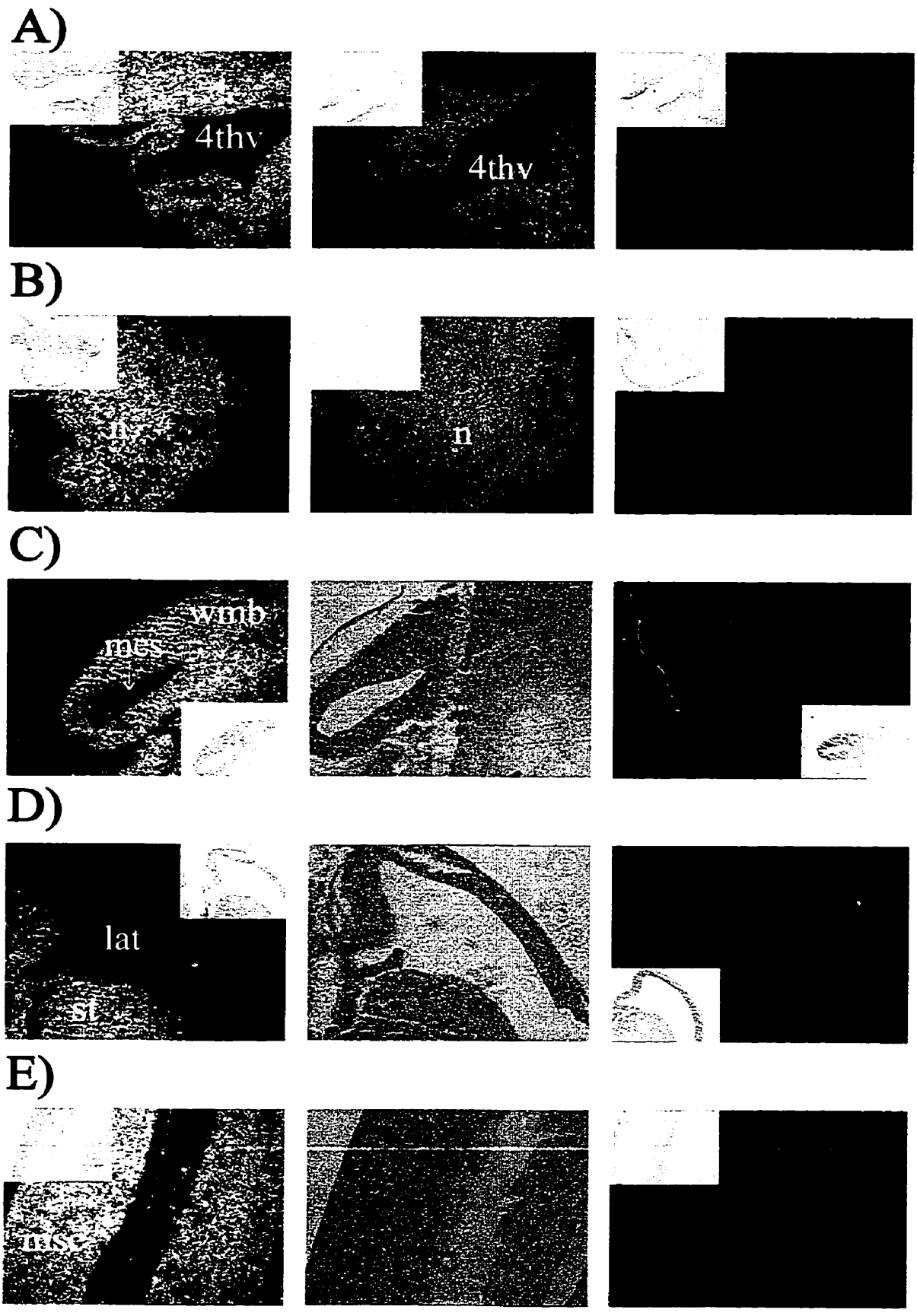
A)
4thv
4thv
B)
n
n
C)
wmb
mes
D)
lat
E)

effort to confirm the results seen in the whole mount *in situ* hybridization experiments, thicker sections were hybridized with the *Naip* probes under the same conditions as their six-micron counterparts. In E13.5 mouse embryo sections, *Naip* transcripts were detected in the tissues surrounding the fourth ventricle (Figure 12A), in the nasal epithelium (Figure 12B), in the wall of the midbrain (Figure 12C), in the striatum and the cells neighboring the lateral ventricle (Figure 12D). DIG-*Naip* antisense labeled probes mirrored the results obtained with the ^{33}P labeled probes (Figure 12 C, D and E, center panels). *Naip* RNA was also identified in the mantle layer of the spinal cord (Figure 12 E) as seen in the whole mount hybridization experiments (Figure 5B). *Naip* antisense labeling of transverse sections through the medulla oblongata, in the rostral spinal cord, established the presence of *Naip* transcripts in the mantle layer (Figure 13A). This pattern was also observed in more rostral transverse sections where *Naip* RNA was again identified in the mantle layer of the spinal cord but also in the dorsal root ganglia and the notochord (Figure 13B). Figure 13C reveals the presence of *Naip* transcripts in cells surrounding the residual lumen of the anterior lobe of the pituitary (previously the Rathke's pouch) while Figure 13D demonstrated *Naip* RNA in olfactory epithelium of the nasal cavity of antisense labeled transverse sections through the head. Sagittal sections (Figure 13E) and transverse sections (Figure13F) through the liver of E13.5 mouse embryo labeled with antisense *Naip* riboprobe show the presence of the genes transcripts in this tissue.

Naip transcripts were still present in the roof of the midbrain, the cells surrounding the mesencephalic vesicle (Figure 14A), the roof of the neopallial cortex (Figure 14B) in antisense probed sagittal section of E14.5 mouse embryos. The lip

Figure 13: ^{33}P *in situ* hybridization of transverse and sagittal sections of E13.5 mouse embryos hybridized with a 1038 base pair *Naip* probe. Panels on the left are the dark field exposures of the *Naip* antisense labeled probes while those on the right are the sense labeled sections. Insets are the respective light field exposure when available. A) Transverse section through upper head region of E13.5 mouse embryo showed *Naip* to be present in the mantle layer of the spinal cord (sc) (x10). B) Transverse sections through the medulla oblongata revealed *Naip* transcripts in the mantle layer of the spinal cord (msc), the dorsal root ganglia (drg) and the notochord (ntc) (x10). C) And D) In transverse sections through the head, *Naip* was found in a vestigial structure of the Rathke's pouch (R) as well as in the developing nasal epithelium (x10). E) And F) Sagittal and transverse sections trough the liver (li) expressed *Naip* (x10). Optic chiasma (oc), olfactory epithelium (oe), abdominal wall (aw).

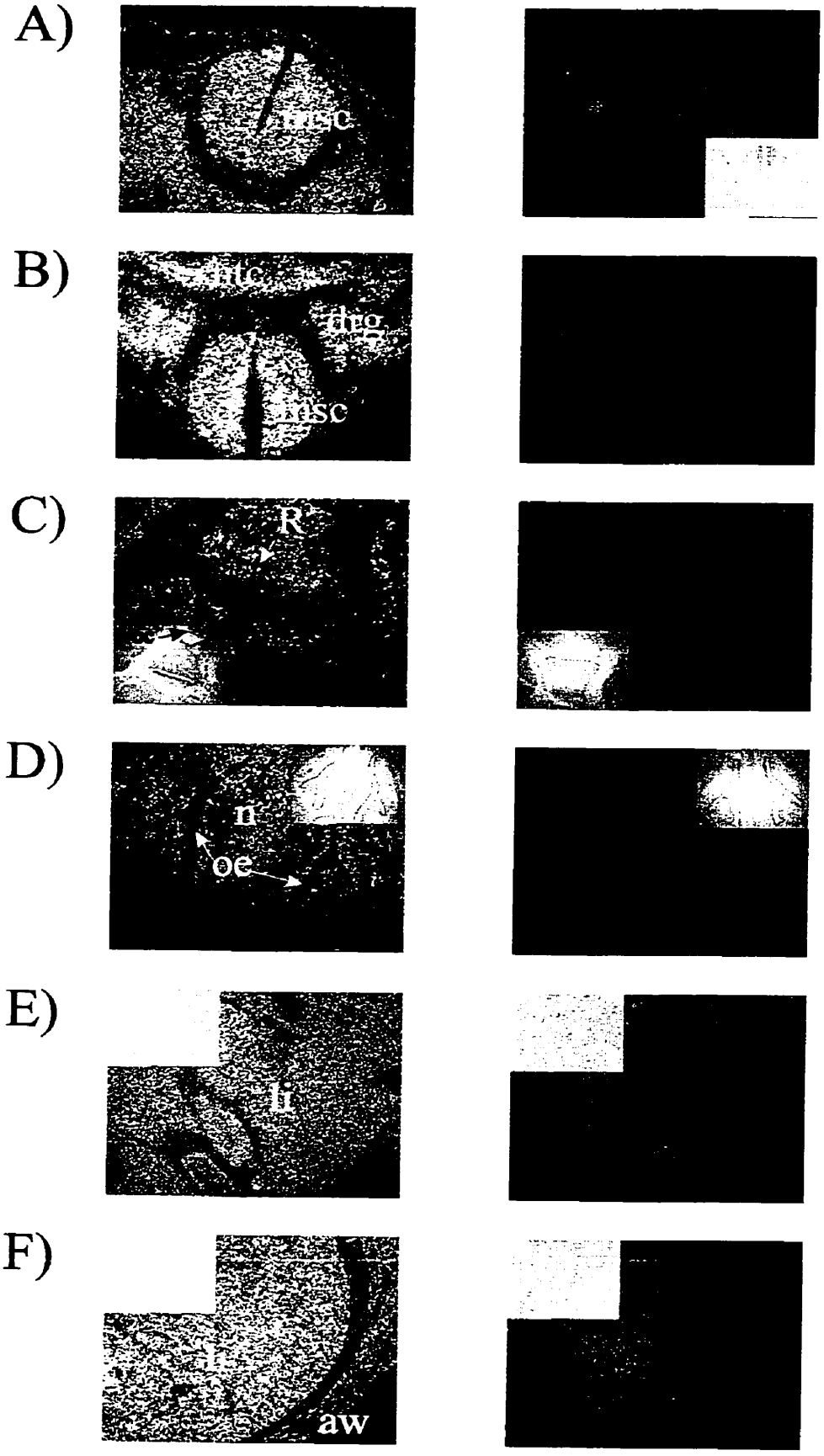
A)
B)
C)
D)
E)
F)
R
n
oe
aw

Figure 14: *in situ* hybridization of transverse and sagittal sections of E14.5 mouse embryos hybridized with a 1038 base pair *Naip* probe. Panels on the left are the dark field exposures of the *Naip* antisense labeled probes while those on the right are the sense labeled sections. Insets are the respective light field exposure when available. Sagittal sections through the head region of E14.5 mouse embryo showed *Naip* to be present in the roof of the midbrain (rmb)(A), the neopallial cortex (nc) of the lateral ventricle (B) and in the developing lip area (C)(x10). Sagittal sections through the body probed with a ^{33}P *Naip* antisense probe, revealed transcripts in the mantle layer of the spinal cord (msc)(D) while no signal was detected in the heart (h). (E) (x10). Transverse sections through the head of the E14.5 mouse embryos labeled with ^{33}P *Naip* antisense probe, again demonstrated *Naip* to be present in the mantle layer of the spinal cord (F) as well as in the neural layer of the retina (nr)(G) (x10). H) *Naip* was detected in the developing intestine with an antisense DIG-labeled probe (x10).

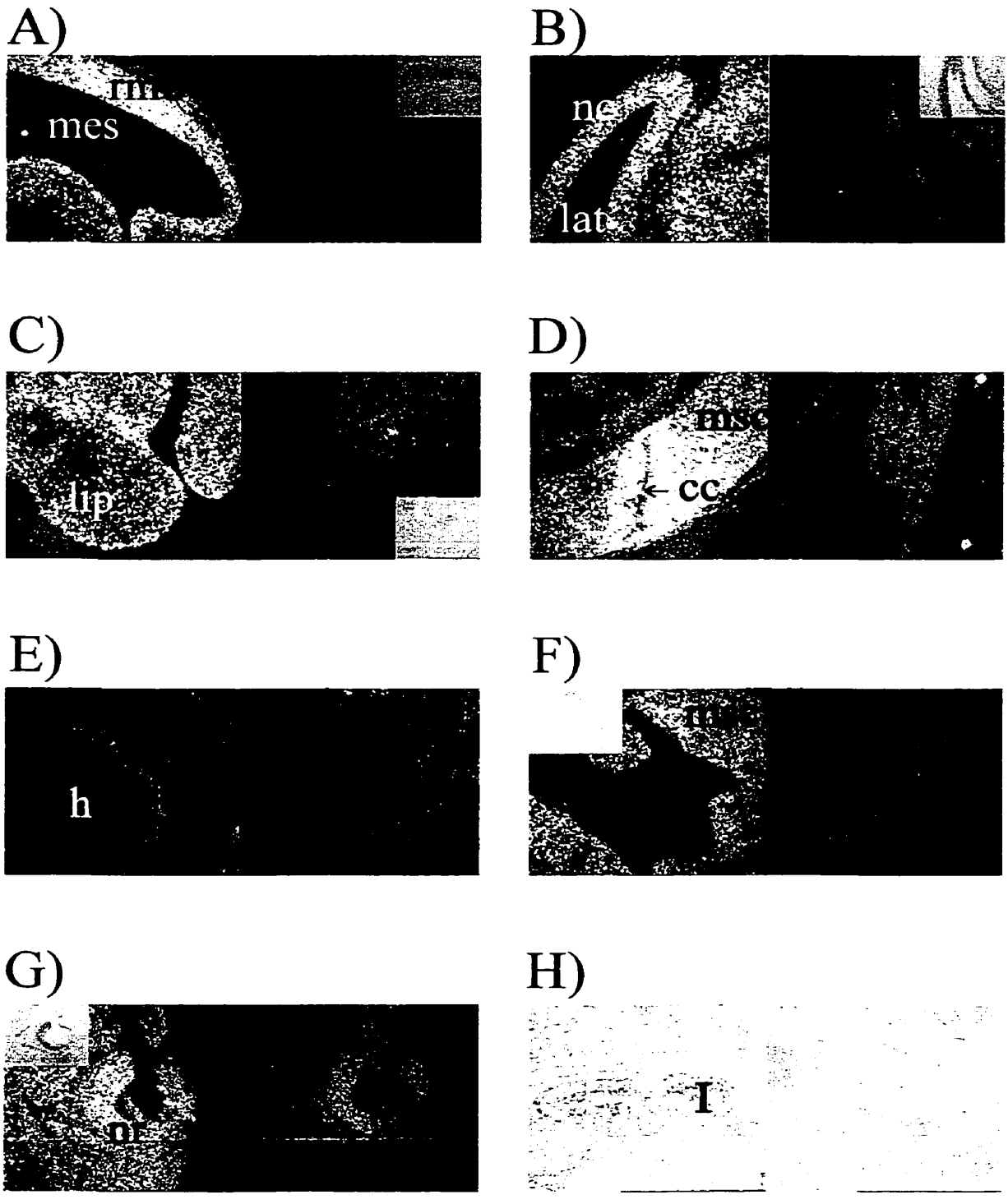
A)
mes
B)
ne
lat
C)
lip
D)
cc
E)
h
F)
G)
n
H)
I

(Figure 14C) as well as the mantle layer of the spinal cord (Figure 14D) was also shown to express *Naip*. The heart of E14.5 mouse embryos did not display the presence of Naip RNA (Figure 14E). Transverse sections at the level of the eye of E14.5 mouse embryos labeled with *Naip* antisense riboprobe revealed the presence of the *Naip* message in the spinal cord (Figure 14F), the neural layer of the retina (Figure 14G). DIG-*Naip* antisense labeled probes revealed the presence of transcripts in the developing intestinal tissue of E14.5 embryos (Figure 14H).

E16.5 mouse embryos labeled with antisense *Naip* riboprobe had a very different pattern of gene expression. The neopallial cortex composed of the cortical plate and the marginal zone of the lateral ventricle expressed Naip RNA (Figure 15A). Sagittal sections of E16.5 embryos labeled with ^{33}P antisense *Naip* probe (Figure 15-1) or with a DIG-*Naip* antisense probe (Figure 15-3) revealed its presence in the lip and primordia of follicles of vibrissae associated with the lip. The epithelial cells of the intestinal villi expressed *Naip* as seen with a ^{33}P antisense *Naip* probe (Figure 15C-1) and with a DIG-*Naip* antisense probe (Figure 15C-4). The neural layer of the retina as well as the developing lenses were strongly labeled by *Naip* antisense probe (Figure 15D). In the spinal cord of E16.5 mouse embryos no labeling was seen with the *Naip* antisense riboprobe (Figure 15E).

Figure 15: *in situ* hybridization of E16.5 sagittal mouse embryo sections with a *Naip* probe. A) 1- ^{33}P silver grain dark field antisense expression of *Naip* in the marginal zone (mz) of the lateral ventricle of the brain (x10). Next panels are respectively, the light field, toluidine blue counter-stained ^{33}P antisense-labeled section (2), the ^{33}P dark field sense labeled micrograph (3) and its light field counterpart (4) (x10). B) 1- in the upper lip area, ^{33}P antisense *Naip* silver grain dark field micrographs showed the transcripts to be present in the primordia follicles of the vibrissae (v) when compared to the sense labeled dark field micrographs (2). Inset to Figure B-1 is the light field exposure of the ^{33}P antisense labeled section. B-3 results from the labeling with a DIG-antisense labeled probe also showing vibrissae staining (x10). C) 1- Dark field micrograph of the ^{33}P antisense *Naip* labeled section-showing expression in the intestinal epithelium (i). 2- light field micrograph of the ^{33}P antisense *Naip* labeled section showed in C1. 3- Dark field micrograph of the ^{33}P sense *Naip* labeled section-demonstrating absence of signal. 4- section from the labeling with a DIG-antisense labeled probe also showing intestinal epithelium staining. Inset, DIG-sense labeled section (x10). D) Dark field micrograph of ^{33}P antisense *Naip* labeled eye section showing distribution in the neural layer of the retina (nr) as well as in the lens (ls). The *Naip* sense probe did not show any staining. Insets are the respective light field micrographs (x10). E) Dark field micrograph of ^{33}P *Naip* antisense-labeled spinal cord did not detect the presence of *Naip* when compared to the sense labeled section (left panel)(x10).

A)

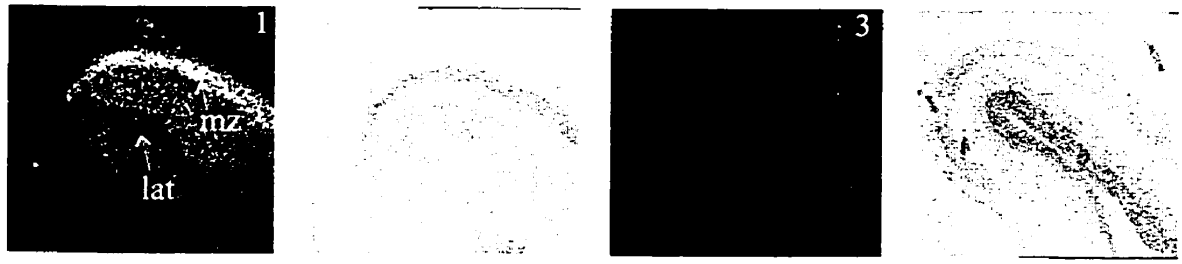

B)

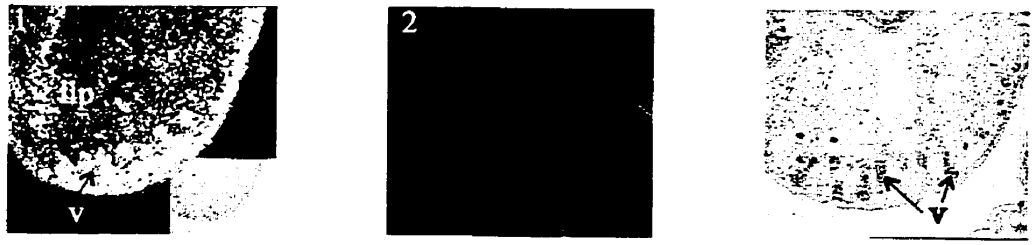

C)

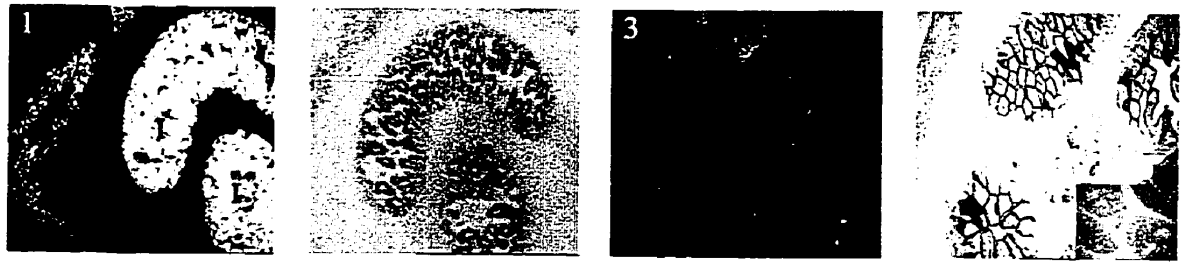

D)

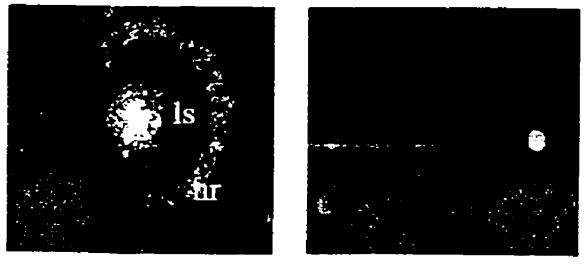

E)

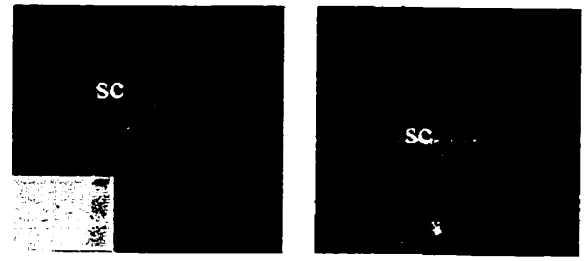

	E9.5	E10.5	E11.5	E12.5	E13.5	E14.5	E16.5
Forebrain							
Telencephalon	+	+	+				
Lateral Ventricle				+	+	+	+
Diencephalon[1]					+		
Third ventricle				+			
Midbrain							
Mesencephalon	+	+	+	+	+	+	
Wall of the midbrain				+	+	+	
Hindbrain							
Met- and Mylencephalon					+		
Fourth Ventricle	+	+	+	+	+		
Medulla oblongata				+			
Branchial Arches	+	+	+				
Spinal cord		+	+	+	+	+	-
Neural tube	+	+	+				
Dorsal Root Ganglia			+	+	+		
Nasal epithelium			+	+	+	+	+
Eye							
Retina					+	+	+
Lens							+
Gastrointestinal system							
Intestinal villi						+	+
Liver			+	+	+		
Cardiovascular system							
Heart			-			-	
Limbs		+					
Future Digits				+			

Table 5: Summary of the distribution of *Naip* transcripts during murine embryogenesis. Presence of signal is indicated as (+) and absence of signal is indicated as (-).

4. DISCUSSION

Naip is expressed at low levels throughout the developing mouse

In keeping with previous reports, the data presented here shows that even in the embryo, the overall expression of *Naip* is low, as 60 cycles of PCR were needed to visualize any amplification product. The presence of *Naip2* during murine embryogenesis was confirmed by the use of primers specific for this locus. This is the only *Naip* copy whose expression was verified in this study as all other primer pairs used amplified *Naip1*, *Naip 2* and *Naip 3* and possibly the remaining *Naip* loci. *Naip1* specific primers were used to try and determine if the neuronal copy of *Naip* is expressed during murine embryogenesis however, this experiment failed. This may have occurred because of very low levels of expression of *Naip1* at the stages examined. The low abundance of *Naip1* is probably due to the fact that the copy of this gene is not critical during development as proven by *Naip 1* (-/-) knock out mice, which are viable with no developmental CNS abnormalities (Dr. M. Holcik, personal communications). However, there is an increase in the cell death of the CA3 neurons of the hippocampus of the *Naip 1* (-/-) mice after administration of kainic acid (Dr. M. Holcik, personal communications). No significant difference was seen in the RT-PCR products from various developmental periods suggesting that the level of *Naip* expression is low in all stages examined.

Detection of *Naip* transcripts using whole-mount *in situ* hybridization

In this study, we present data on the expression of *Naip* during murine embryogenesis. The whole mount *in situ* hybridization analysis revealed an expression pattern for *Naip* during development. Unfortunately this method did not allow us to

delineate which copies of *Naip* were being expressed during the embryo's development as attempts to hybridize with *Naip1* or *Naip2* specific probes failed. This could have been a result of the absence of the *Naip1* copy but this is not true of the *Naip2* copy as its presence was documented by RT-PCR (figure 2C). The absence of signal was more likely due to an inability for the probe to properly bind to its target or to a very low expression, which could not be visualized by the DIG whole mount *in situ* hybridization method.

In view of the low levels detected for *Naip* by RT-PCR, a number of parameters were tested to optimize the DIG whole mount *in situ* hybridization method. Among these were the incubation time in proteinase K, the nature of the blocking agent used prior to hybridization with the DIG antibody and the ratio of the substrates. These parameters were analyzed in order to obtain staining with the least amount of background while preserving the integrity of the embryos structures. For example the ratio of NBT/BCIP was varied. Most published reports employ a 1:1.9 ratio of BCIP/ NBT. In accordance with Arcellana-Panlilio and Schultz (1994) we found that omission of NBT greatly reduced the level of background although increasing the time required for the colorimetric reaction to take place. To circumvent this problem we used a 1:0.9 ratio of BCIP/NBT allowing a better control over the rate at which the colour developed. We also found that background levels varied from sample to sample as well as with the probes utilized.

Once the DIG-*Naip* labeled whole mounts were obtained they were sectioned. Unfortunately these attempts failed, as the signal was always lost. Moreover, sectioning of the embryos prior to hybridization with a DIG-*Naip* labeled probe revealed the presence of *Naip* only in a subset of those structures that were shown to be *Naip* positive

by whole mount *in situ* hybridization. Discrepancies between the analysis of the sectioned slides and the whole mounts may have been the result of the physical limitations of the techniques themselves. For example, signals may have been detected in the whole mounts because of the presence of several layers of DIG-*Naip* positive cells. However, upon sectioning the layering is reduced such that the amount of DIG-*Naip* positive cells present on a section may not be sufficient to be visualized by the DIG technique and would thus be perceived as an absence of signal.

Naip is expressed throughout the developing mouse CNS; primarily in non-apoptotic regions.

Radiolabeled riboprobes were utilized on sectioned embryos in an attempt to delineate the exact *Naip* expressing structures. ^{33}P-UTP was used to label our riboprobes because it allows the detection of low abundance mRNAs with less background than does ^{35}S (Faulkner-Jones, 1993). This method corroborated the pattern observed in the whole mount *in situ* hybridization in that CNS and spinal cord expression was detected in E9.5 to E13.5 sections. Given NAIP protein's previously described expression in the rat central nervous system as well as in the spinal cord, the detection of the mouse *Naip* transcripts in these developing tissues was expected (Xu *et al.*, 1997).

Signals were found at varying levels in the developing CNS in all stages examined suggesting a role for *Naip* in normal brain function and development. E9.5 to E14.5 embryos were found to express *Naip* transcripts in the neuroepithelium of the fourth ventricle, telencephalon and mesencephalon. The expression in the brain of E16.5 embryo sections decreased notably relative to E14.5 expression and was restricted to the cortical and marginal layers of the lateral ventricle. The cortical plate is composed of

post-mitotic cells and plays a decisive role in the organization of the definitive cortex (Naruse and Keino, 1995). In the murine embryonic cortex, dying cells are rare at E10.5 but by E14.5, comprise 70%. This number decreases to 50% by E18.5. The majority of the dying cells are found in proliferative zones rather than in regions of post-mitotic neurons (Blaschke *et al.*, 1996). The expression of anti-apoptotic genes in the developing cortical plate is not uncommon as both Bcl-2 (Novack and Korsmeyer, 1994) and A1 (Carrio *et al.*; 1996) have been localized in these regions at E16.5 of mouse development. The absence of the *A1* and *Bcl-2* transcripts in the highly apoptotic region of the intermediate zone and high expression of the proteins in the proliferative region of the cortex is consistent with a role for these genes in brain development (Carrio *et al.*, 1996). Similarly, *Naip* may be acting as an anti-apoptotic mediator in these important areas of the developing cortex. It may be significant that *Naip* functions in a distinct pathway from that of the *Bcl-2* family members, as it is interacting with and inhibiting Caspase-3 (J.Maier, pers.communications). Studies on the distribution of *Caspase-3* mRNA and activated Caspase-3 protein, as well as the appearance of apoptotic cells in the developing cerebral cortex of E18.5 mice have revealed that *Caspase-3* mRNA was most abundant in the cortical plate while apoptotic cells and activated Caspase-3 protein were both mostly located in the proliferating ventricular zone (Urase *et al.*, 1998). While activation of Caspase-3 is not observed for the death of post-mitotic cells of the cortical plate at E18.5, it is essential in the apoptosis of the neuroepithelium of E10.5-11.5 and undifferentiated proliferative neurons of E18.5 mice (Urase *et al.*, 1998). Given *Naip*'s inhibition of Caspase-3, it is possible that it protects against the activation of this pro-apoptotic caspase in the cells of the cortical plate.

Naip is expressed in the progenitors of the spinal cord.

A central and as yet unanswered question in the molecular pathogenesis of SMA is whether NAIP loss exacerbates the clinical phenotype (Burghes, 1998; MacKenzie, 1998). *Naip* CNS expression was observed from E9.5 to E14.5 in the neuroepithelium of the neural tube and spinal cord. E12.5 and E13.5 hemi-sectioned embryos, which underwent the whole mount *in situ* protocol, revealed the presence of *Naip* in the mantle layer of the spinal cord. This pattern of expression was confirmed with transverse sections through the spinal cord of E13.5 revealing a very disperse expression pattern of the transcript (Figure 13b). The mantle layer of the embryonic spinal cord contains postmigratory and migrating young neurons as well as post-mitotic young neurons and glioblasts eventually becoming the gray matter of the mature spinal cord. Although this study did not permit the precise identification of *Naip* positive cells, it is interesting to consider the implication of the presence of *Naip* in the future anterior horn of the spinal cord with respect to the pathogenesis of SMA.

Given SMN's central role in SMA pathogenesis and the role we propose for NAIP, a comparison of the expression of these two genes is instructive. SMA is characterized by the loss of motor neurons in the anterior horn of the spinal cord and lower brain stem (Towfighi *et al.*, 1985). Battaglia *et al.*, (1997) and Tizzano *et al.*, (1998) have shown that SMN, the SMA causative gene, is expressed in the very cells affected in SMA. Tizzano's *et al* (1998) demonstration of the presence of *SMN* in the spinal cord of both the human fetus and adult as well as in the adult cortex is consistent with a role for SMN in normal neuron ontogenesis and maintenance. Battaglia's *et al.*, (1997) study of SMN distribution during rat and monkey development revealed different

levels of SMN expression among different motor neurons. They suggest that the differences in expression levels might explain the survival of the motor neurons in the milder forms of SMA. As *SMN2* can generate full-length SMN, it rescues the neuropathic effect of *SMN1* deletion thus modulating the severity of SMA (Lefebvre *et al*, 1997). Correlation has been made between the copy number of *SMN2* and SMA severity but we cannot exclude the possibility of the existence of other modifying genes as patients with similar number of SMN2 exhibit variations in their phenotype (Lorson *et al*, 1998; Scharf *et al*., 1998). The presence of *Naip* transcripts in the developing spinal cord aids in implicating this gene in the pathogenesis of SMA.

Furthermore the course of SMA suggests early losses of functioning in motor neurons followed by increases in the stability of surviving motor neurons (Crawford and Pardo, 1996). This has led to the idea that SMA is a disease resulting from defects in the apoptosis seen during development (Sarnat 1984, Oppenheim, 1991). During normal human development, motoneuron loss occurs between 11 weeks and 25 weeks of gestation with the greatest decline occurring between 12 and 16 weeks (Forger and Breedlove, 1987). We have witnessed *Naip*'s expression during murine embryo spinal cord formation to be at its peak at the time where motor neuron loss should be at its greatest, that is with the zenith of motor neuron cell death occurring at E14 (Lance-Jones, 1982). *Naip* mRNA expression in the spinal cord was very strong until E14.5 and became undetectable at E16.5. Whether or not *Naip* has an antiapoptotic function during the second trimester of gestation remains to be studied but it is apparent that it does have a role in spinal cord development. The drop in the level of *Naip* transcript expression in the

spinal cord, early in the third trimester of gestation, was not surprising as previous studies had documented *NAIP* levels to be low in the adult human spinal cord (Roy *et al;* 1995).

Naip is expressed in other tissues involved in SMA such as the dorsal root ganglia

In addition to motorneurons, attrition of dorsal root ganglia is also seen in SMA. Neuropathological studies from various groups have documented ballooned neurons and chromatolytic neurons in the dorsal root ganglia of some type I SMA patients despite the absence of detectable clinical sensory abnormalities in SMA (Murayama *et al.*, 1991; Towfighi *et al.*, 1985). *SMN* has been documented in the dorsal root ganglia (Tizzano *et al*; 1998). Likewise, *Naip* transcripts were also found in the dorsal root ganglia, indicating that *Naip* is also expressed in the peripheral nervous system. The implication of *Naip* and SMN presence in the dorsal root ganglia with regard to SMA is still unclear however it suggests that they have a role in the development of the sensory neurons.

Naip transcripts showed a uniform expression in the dorsal root ganglia of E11.5 mouse embryos that continued in E13.5 embryos. Similarly, *Caspase-3* mRNA showed strong and uniform expression in the dorsal root ganglia of E11.5 mouse embryos whereas activated Caspase-3 positive cells showed a more restricted pattern of expression which coincided with the spatio-temporal appearance of apoptotic cells (Urase *et al*, 1998). Activation of Caspase-3 proteases causes apoptosis of DRG neurons (Mukasa *et al;* 1997) and *Naip*'s involvement in promoting the survival of neurons in the dorsal root ganglia, with respect to caspase mediated cell death, will only be clarified with a study on the distribution of Naip protein with in this tissue.

Naip message is expressed in other tissues not affected in SMA

The nasal epithelium and the developing eye are two other sensory areas where *Naip* transcripts were found. In the nasal area *Naip* expression was always diffuse until E16.5 at which stage it is found in the primordia of follicles of vibrissae associated with the lip. *Naip* transcripts were found in the neural layer of the retina as well as in the lens of the embryos from E11.5 to E16.5. Both the olfactory epithelium as well as the developing retina are organs that undergo cell death during their development (Capello *et al*, 1999;Young, 1984). Cell death in the retina of the mouse occurs during the first two weeks after birth, while programmed cell death has been reported in the nasal placode epithelium from as early as E10.5 (Grindley *et al;* 1995, Young, 1984). The function of *Naip* in these tissues remains unclear.

Naip was also localized in the first and second mandibular component of the branchial arch of E11.5 embryos. During development, cells migrate and proliferate around the pharynx, and meet the opposite arch (Craigmyle and Presley, 1975). The ectoderm covering the branchial arches is one of the cell types involved in the initial fusion between the arches however, this cell population is absent from the fusion zone and one of the proposed mechanism for removal of the epithelia cells is programmed cell death (Shuler, 1995). Our data does not allow the identification of which cell type of the developing mandibular arch is *Naip* positive but when considering the tendency for apoptosis in that area it is possible to postulate a role for *Naip*.

Results from both *in situ* hybridization techniques were also concordant in the developing future digits of E12.5 mouse embryo hindlimbs (Figure 4E and Figure 11D). The cell death of the interdigital zones of the developing limbs is a well-characterized

finding. *Naip's* presence in areas in the future digits, an area that is not prone to undergo programmed cell death, is consistent with a role of *Naip* as an antiapoptotic agent. As reported by Novack and Korsmeyer (1994), the anti-apoptotic protein Bcl-2 is also located in the digital zones of E12.5 embryos. They suggests that cells lacking Bcl-2 are susceptible to the cell death signal thus down regulation of Bcl-2 in the interdigital space may be important for the programmed cell death to occur. However Bcl-2 knockout mice have normal limb development thus suggesting that other factors are required for the development of digits. *Naip* may be one such factor.

Naip expression was very high in the developing intestine of E16.5 embryos. At E14.5, the epithelium is undifferentiated but by E16.5, the tissue convolutes with developing villi. *Naip* transcript expression is restricted to the villi unlike Bcl-2, the expression of which is restricted to the progenitor cells at the base of the villi (Novack and Korsmeyer, 1994). *Naip* is once again present in cells that have ceased to divide (Traber, 1994) but which are migrating to the villus tip. Absorptive enterocytes and goblet cells are extruded into the intestinal lumen of the adult mouse (Traber, 1994), an event shown to occur at the tip of the rat villus where apoptotic cuffs are formed in contrast to the mid-villus and crypt cells which are non-apoptotic (Westcarr *et al*, 1999). It is unclear which of the six murine *Naip* loci are expressed in the intestine. Delineation of the protein's role in the intestinal tract will likely be clarified with the identification of the responsible loci and analysis of mouse models null for these gene copies.

Conclusion

Naip has a distinct expression pattern in the developing mouse embryo when compared to other modulators of apoptosis, such as Bcl-2, and to other members of the IAP family such as Survivin (Adida *et al*, 1998). When contemplating *Naip's* phylogenetic relationship to the other BIR containing genes, it is evident that it is in a class by itself (Deveraux and Reed, 1999). While other IAPs members such as XIAP have had a strong inhibition of apoptosis documented or a role in regulating cell proliferation (e.g. Survivin), *Naip* is comparatively distinct at the sequence level and in addition to inhibiting apoptosis it is clearly developmentally regulated. Our data has showed a *Naip* expression pattern of developmental stage-specific expression in various organs of the mouse embryo. Interestingly, some of the tissues where *NAIP* expression has been revealed in the adult such as the lungs and the heart are void of *Naip* during mouse embryogenesis. These data suggest a role for *Naip* in the specialized function of these organs in adults rather than in their development. Other tissues, such as the brain, show low expression throughout adulthood. This involvement of a gene in many tissues other than the one(s) linked to the disease to which the gene is associated is not uncommon in genes involved in neurodegenerative disorders. One such example is Huntington disease gene in the rat where, despite the regional specificity of the degeneration in Huntington's disease, the gene is expressed in organs not implicated in the progression of the disease (Strong *et al*; 1993).

Naip has a widespread expression in various tissues of the body. Some of the *Naip* positive tissues are the tissues that are affected by the very specific pathology of SMA. One model of SMA pathogenesis involves motor neuron attrition in the second and

possibly third trimester of gestation. Our observation of *Naip* transcripts in the spinal cord between E9.5 and E14 .5 (equivalent to the second trimester) is consistent with a role for *Naip* in modifying SMA severity. In some tissues, *Naip's* temporal expression coincides with the onset of programmed cell death. The role of *Naip* in all of the tissues where it was found remains to be elucidated. Our results suggest a developmental regulation of *Naip* expression. While *Naip*'s implication in the pathogenesis of SMA may be due to its developmentally regulated expression, its exact involvement in the pathogenesis of the disease remains to be clarified; comparison of SMN deficient mice with SMN deficient/NAIP null mice will help clarify this issue.

REFERENCES

Adida, C., Crotty, P., McGrath, J., Berrebi, D., Diebold, J., Altieri. 1998. Developmentally regulated expression of the cancer anti- apoptosis gene *survivin* in the human and mouse differentiation. *American J of Pathology.* **152:**43-49.

Ambrosini, G., Adida, C., Altieri, D.C. 1997. A novel anti-apoptosis gene, survivin, expressed in cancer and lymphoma. *Nature Medicine* **3:**917-921.

Ambrosini, G., Chu, E.Y., Plescia, J., Tognin, S., Marchisio, P. C. Altieri,D.C. 1998. Control of apoptosis and mitotic spindle checkpoint by survivin. *Nature* **396:** 580-584.

Arcellana-Panlilio, M.Y., Schultz, G. A. 1994. Temporal and spatial expression of major histocompatibility complex class I H-2K in the early mouse embryo. *Biol Reprod* **51:**169-183.

Battaglia, G., Princivalle, A., Forti, F., Lizier,C., Zeviani, M. 1997. Expression of the *SMN* gene, the spinal muscular atrophy determinating gene, in the mammalian central nervous system. *Human Molecular Genetics* **6:**1961-1971.

Bergin, A., Kim, G., Price, D., Sisodia, S. S., Lee, M. K., Rabin, B. A. 1997. Identification and characterization of a mouse homologue of the spinal muscular atrophy-determining gene. *Gene.* **204:**47-53.

Blaschke, A. J., Staley, K., Chun, C. 1996. Widespread programmed cell death in proliferative and postmitotic regions of the fetal cerebral cortex. *Development* **122:**1165-1174.

Brooke, M.H.1985. *A clinician's view of neuromuscular disorders.* (Williams and Wilkins, London), 2nd Ed., pp. 36-80.

Boehringer Mannheim. 1996. *Nonradioactive In Situ Hybridization Application Manual.* 2nd ed. Edited by S. Grunewald-Janho, J. Keesey, and M. Leous. Printed in Germany. pp 8-56.

Boise, L. H., Gonzales-Garcia, M., Postema, C. E., Ding, L., Lindsten, T., Turka, L. A., Mao, X., Nunez, G., Thompson, C. B. 1993. *bcl-x*, a *bcl-2* related gene that functions as a dominant regulator of apoptotic cell death. *Cell* **74:**597-608.

Brzustowicz, L. M., Lehner, T., Castilla, L. H., Penchaszadeh, G. K., Daniels, R., Davies, K. E., Leppert, M., Ziter, F., Wood, D., Dubowitz, V., Zerres, K., Hausmanowa-Petrusewicz, I., Ott, J., Munsat, T. L., Gilliam, T.C.1990. Genetic mapping of chronic childhood-onset spinal muscular atrophy to chromosome 5q11.2-q13.3. *Nature* **344:**540-541.

Burghes, A. 1998. Reply to MacKenzie. *Am J Hum Genetic* **62:**486-488.

Burglen, L., Lefebvre, S., Clermont, O., Burlet, P., Viollet, L., Cruaud, C., Munnich, A., Melki, J. 1996. Structure and organization of the human survival motor neurone (SMN) gene. *Genomics* **32:**479-482.

Burlet, P., Burglen, A., Clermont. O., Lefebvre, S., Viollet, L., Munnich, A. Melki, J. 1996. Large-scale deletions of the 5q13 regions are specific to Werdnig-Hoffmann disease. *J. Med. Genet.* **33:**282-283.

Burlet, P., Huber, C., Bertrandy, S., Ludosky, M., Zwaenepoel, I., Clermont, O. Roume, J., Delezoide, A., Cartaud, J., Munnich, A., Lefebvre, S. 1998. The distribution of SMN protein complex in human fetal tissues and its alteration in spinal muscular atrophy. *Hum. Mol. Gen.* **7:**1927-1933.

Campbell, L., Potter, A., Ignatius, J., Dubowitz, V., Davies, K. 1997. Genomic variation and gene conversion in spinal muscular atrophy: implications for disease process and clinical phenotype. *Am J Hum Genet* **61:**40-50.

Cappello, P., Tarazzo, G., Benedetto, A., Fasolo, A. 1999. Proliferation and apoptosis in the mouse vomeronasal organ during ontogeny. *Neurosci Lett.* **266:**37-40.

Carrio,R., Lopez-Hoyos, M., Jimeno, J., Benedict, M., Merino, R., Benito, A., Fernandez-Luna, J., Nunez, G., Garcia-Porrero, Merino, J. 1996 *A1* Demonstrates restricted tissue distribution during embryonic development and functions to protect against cell death. *American Journal of Pathology* **149:**2133-2142.

Cecconi, F., Alvarez- Bolado, G., Meyer, B. I., Roth, K. A., Gruss, P. 1998. Apaf-1 (ced-4 homolog) regulates programmed cell death in mammalian development. *Cell* **94:**727-737.

Chen, Q. Baird, S., Mahadevan, M., Besner- Johnston, A., Farahani, R., Xuan, J., Kang, X., Lefebvre, C., Ikeda, J. E., Korneluk, R.G., MacKenzie, A. 1998. Sequence of a 131-kb region containing the spinal muscular atrophy candidate genes SMN and NAIP. *Genomics.* **48**:121-127.

Chittenden, T., Harrington, E. A., O'Connor, R., Flemington, C., Lutz, R. J., Evan, G. I., Guild, B. C. 1995. Induction of apoptosis by the Bcl-2 homologue Bak. *Nature* **374:**733-736.

Chou, S.M., Fakadej, A.V. 1971. Ultrastructure of chromatolytic motorneurons and anterior spinal roots in a case of Werdnig-Hoffmann disease. *J Neuropathol Exp Neurol* **30:**368-379.

Cowan, W.M., Fawcett, J. W., O'Leary, D. M., Stanfield, B. 1984. Regressive events in neurogenesis. *Science* **225:**1258-1265.

Craigmyle, M., Presley, R. 1975. *Embryology*. Second edition. Bailliere Tyndall. London. Pp.126-127.

Crawford, T. O. 1996. From enigmatic to problematic, the new molecular genetics of childhood spinal muscular atrophy. *Neurology* **46:**335-340.

Crawford, T. O., Pardo, C.A. 1996. The neurobiology of childhood spinal muscular atrophy. *Neurobiol Dis.* **6:**397-408.

Deveraux,Q. L., Reed, J.C. 1999. IAP family proteins: suppressors of apoptosis. *Genes Dev.* **13:**239-252.

Deveraux, Q. L., Takahashi, R., Salvesen, G. S., Reed, J.C. 1997. X-linked IAP is a direct inhibitor of cell-death proteases. *Nature* **388:**300-304.

Devriendt, K., Lammens, M., Schollen, E., Van Hole, C., Dom, R., Devlieger, H., Cassiman, J., Fryns, J., Matthjs, G. 1996. Clinical and molecular genetic features of congenital spinal muscular atrophy. *Ann Neurol.* **40:**731-738.

DiDonato, C., Chen, X., Noya, D., Korenberg, J., Nadeau, J., Simard, L. 1997. Cloning, characterization and copy number of the murine survival motor neuron gene: homolog of the spinal muscular atrophy-determining gene. *Genome Res.* **7:**339-352.

Dubowitz, V. 1995. *Muscle Disorders in Childhood*, 2nd ed. London, Philadelphia: Saunders.

Ellis, R. E., Yuan, J., Horvitz, H. R. 1991. Mechanisms and functions of cell death. *Annu Rev Cell Biol* **7:**663-698.

Fadeel, B., Zhivotovsky, B., Orrenius, S. 1999 All along the watchtower: On the regulation of apoptosis regulators. *FASEB Journal.* **13:**1647-1657.

Faulkner-Jones, B.E. 1993 ^{33}P: advantages for *in situ* hybridization. *Amersham Life Science.* **11:**5-6.

Fidzianska, A., Goebel, H. H., Warlo, I. 1990. Acute infantile spinal muscular atrophy. Muscle apoptosis as a proposed pathogenetic mechanism. *Brain* **113:**433- 445.

Fidzianska, A., Hausmanowa-Petrusewicz, I. 1984. Morphology of the lower motor neuron and muscle. In: *Progressive Spinal Muscular Atrophies.* Edited by I. Gamstrop and H. B. Sarnat, New York: Raven Press, pp. 55-89.

Fischer, U., Liu, Q., Dreyfuss, G. 1997. The SMN-SIP1 complex has an essential role in spliceosomal snRNP biogenesis. *Cell* **90:**1023-1029.

Forger, N., Breedlove, M. 1987. Motoneuronal death during human fetal development. *J of Comparative Neurology.* **264:**118-122.

Galli-Resta, L., Ensini, M. 1996. An intrinsic time limit between genesis and death of individual neurons in the developing ganglion cell layer. *J.Neuros.* **16:**2318-2324.

Gendron, N. H., MacKenzie, A.E. 1999. Spinal muscular atrophy: molecular pathophysiology. *Current Opinion in Neurology.* **12:**137- 142.

Gillardon, F., Zimmerman, M., Uhlmann, E., Krajewski, S., Reed, J. C., Klimasschewski, L. 1996. Antisense oligodeoxynucleotides to bax mRNA promotes survival of rat sympathetic neurons in culture. *J Neuros Res* **43:**726-734.

Gilliam, T. C., Brzustowicz, L. M., Castilla, L. H., Lehner, T., Penchaszadeh, G. K., Daniels, R. J., Byth, B. C., Knowles, J., Hislop, J. E., Shapira, Y. Dubowitz, V., Munsat, T. L., Ott, J., Davies, K. E. 1990. Genetic homogeneity between acute and chronic forms of spinal muscular atrophy. *Nature* **345:** 823-825.

Grindley, J. C., Duncan, R., Hill, R. E. 1995. The role of *Pax-6* in eye and nasal development. *Development* **121:**1433-1442.

Guettier-Sigrist, S., Coupin, G., Braun, S., Warter, J. M., Poindron, P. 1998. Muscle could be the therapeutic target in SMA treatment. *J. Neurisci. Res.* **53:**663-669.

Hausmanowa-Petrusewicz, I., Fidzianska, A. 1974. Spinal muscular atrophy: fetal- like histopathological pattern in Werdnig- Hoffman disease. *Bulletin of the New York Academy of Medicine.* **50:**1157-1172.

Hausmanowa-Petrusewicz, I., Fidzianska, A., Niebroj-Dobosz, I., Strugalska, M.H., 1980. Is Kugelberg-Welander spinal muscular atrophy a fetal defect? *Muscle Nerve* **3:**389-402.

Hengartner, M. O., Ellis, R. E., Horvitz, H. R. 1992. *C. elegans* gene *ced-9* protects cells from programmed cell death. *Nature* **356:** 494-499.

Hengartner, M. O., Horvitz, H. R. 1994. *C. elegans* cell survival gene *ced-9* encodes a functional homolog of the mammalian proto-oncogene Bcl-2. *Cell* **76:** 665-676.

Hetts, S. W. 1998. To Die or not to die: An overview of apoptosis and its role in disease. *JAMA.* **279:**300-307.

Homma, S., Yaginuma, H., Oppenheim, R. W. 1994. Program cell death during the earliest stages of spinal cord development in the chick embryo: a possible means of early phenotypic selection. *J Comp Neurol.* **345:**377-395.

Jacobson, M., Weil, M., Raff, C. 1997. Programmed cell death in animal development. *Cell* **88:**347-354.

Kamada, S., Shimono, A., Shinto, Y., Tsujimura, T., Noda, T., Kitamura, Y., Kondoh, H., Tsujimoto, Y. 1995. *Bcl-2* deficiency in mice leads to pleiotropic abnormalities: accelerated lymphoid cell death in thymus and spleen, polycystic kidney, hair hypopigmentation, and distorted small intestine. *Cancer res.* **55:**354-359

Kaufman, M. H. 1994. *The Atlas of Mouse Development.* Academic Press, Inc. San Diego CA.

Kerr, J.F., Wyllie, A.H., Currie,A. R. 1972. Apoptosis: a basic phenomenon with wide-ranging implications in tissue kinetics. *Br J Cancer.* **26:**239-257.

Krajewski, S., Krajewska, M., Shabaik, A., Wang, H., Iric, S., Fong, L., Reed, J. C. 1994. Immunohistochemichal analysis of *in vivo* patterns of bcl-x expression. *Cancer Research.* **54:**5501-5507.

Kuida, K., Haydar, T. F., Kuan, C. Y., Taya, C., Karasuyama, H., Su, M. S., Rakic, P., Flavell, R., A. 1998. Reduced apoptosis and cytochrome-c mediated caspase activation in mice lacking caspase-9. *Cell* **94:**325-337.

Kumar, S. 1999. Mechanisms mediating caspase activation in cell death. *Cell Death Differentitation.* **6:**1060-1066.

La Bella, V., Cisterni, C., Salaun, D., Pettmann, B. 1998. Survival motor neuron (SMN) in rat is expressed as different molecular forms and is developmentally regulated. *Eur. J. Neurosc.* **10:**2913-2923.

LaCasse, E. C., Baird, S., Korneluk, R.G., MacKenzie, A. 1998. The inhibitors of apoptosis (IAPs) and their emerging role in cancer. *Oncogene.* **17:** 3247-3259.

Lance-Jones, C. 1982. Motorneuron cell death in the developing lumbar spinal cord of the mouse.*Dev Brain Res* **4:**473-479.

LeBrun, D. P., Warnke, R. A., Cleary, M. 1993. Expression of bcl-2 in fetal tissues suggests a role in morphogenesis. *American J of Pathology.* **142:**743-753.

Lefebvre, S., Burglen, L., Reboullet, S., Clermont, O., Burlet, P., Viollet, L., Benichou, B., Cruard, C., Millasseau, P., Zeviani, M., Le Paslier, D., Weissenbach, J., Munnich, A., Melki, J. 1995. Identification and characterization of a spinal muscular atrophy-determining gene. *Cell* **80:**155-165.

Lefebvre, S., Burlet, P., Liu, Q., Bertrandy, S., Clermont, O., Munnich, A. Dreyfuss, G., Melki, J. 1997. Correlation between severity and SMN protein level in spinal muscular atrophy. *Nat. Gen.* **16:**265-269.

Liston, P., Roy, N., Tamai, K., Lefebvre, C., Baird, S., Cherton-Horvat, G., Farahani, R., McLean, M., Ikeda, J. E., MacKenzie, A., Korneluk, R.G. 1996. Suppression of apoptosis in mammalian cells by NAIP and a related family of IAP genes. *Nature* **379:**349-353.

Liu, Q., Fischer, U., Wang, F., Dreyfuss, G. 1997. The spinal muscular atrophy disease gene product, SMN, and its associated protein SIP1 are in a complex with spliceosomal snRNP proteins. *Cell* **90:**1013-1021.

Lorson, C. L., Strasswimmer, J., Yao, J.M., Baleja, J. D., Hahnen, E., Wirth, B., Le, T., Burghes, A.H., Androphy, E.J. 1998. SMN oligomerization defect correlates with spinal muscular atrophy severity. *Nat Genet* **19:**63-66.

MacKenzie, A. E. 1998. Reply to Burghes. *Am J Hum Genet.* **62:**485-488.

Martinou, J. C., Frankowski, H., Missotten, M., Martinoui, I., Potier, L., Dubois-Dauphin, M. 1994. Bcl-2 and neuronal selection during development of the nervous system. *J. Physiol.* **88:**209-211.

Mathan, M., Moxey , P. C, Trier, J. S. 1976. Morphogenesis of fetal rat duodenal villi. *Am J Anat.* **146:**73-92.

Melki, J., Sheth, P., Abdelhak, S., Burlet, P., Bachelot, M. F., Lathrop, M. G., Frezel, J., Munnich, A. 1990. Mapping of acute (type I) spinal muscle atrophy to chromosome 5q12-q14. The French Spinal Muscular Atrophy Investigators. *Lancet.* **336:**271-273.

Melki, J., Abdelhak, S., Sheth, P., Bachelot, M. F., Burlet, P., Marcadet, A., Aicardi, J., Barois, A., Carriere, J. P., Fardeau, M., Fontan, D., Ponsot, G., Billette, T., Angelini, C., Barbosa, C., Ferriere, G., Lanzi, G., Ottoloini, A., Babron, M. C. 1990. Gene for chronic proximal spinal muscular atrophies maps to chromosome 5q. *Nature* **344:**767-768.

Morrison, K. E. 1996. Advances in SMA research: review of gene deletions. *Neuromusc Disord* **6:**397- 408.

Mukasa, T., Urase, K., Momoi, Y. M., Kimura, I., Momoi, T. 1997. Specific expression of CPP32 in sensory neurons of mouse embryos and activation of CPP32 in the apoptosis induced by withdrawal of NGF. *Biochem. Biophys. Res. Commun.* **231:**770-774.

Murayama, S., Bouldin, T.W., Suzuki, K.1991. Immunocytochemical and ultrastructural studies of Werdnig-Hoffmann disease. *Acta Neuropathol.* **81:**408-417.

Naruse, A., Keino, H. 1995. Apoptosis in the developing CNS. In *Progress in Neurobiology* **47:**135-155.

Newton, K., Strasser, A. 1998. The Bcl-2 family and cell death regulation. *Current Opinions in Genetics and Development.* **8:**68-75.

Nicotera, P., Leist, M., Single, B., Volbracht, C. 1999. Execution of apoptosis: Converging or diverging pathways? *Biological Chemistry* **380:**1035-1040.

Novack, V. D., Korsmeyer, S. 1994. Bcl-2 protein expression during murine development. *American J of Pathology.* **145:**61-73.

Oltvai, Z. N., Korsmeyer,J., 1994. Checkpoints of dueling dimers foil death wishes. *Cell* **79:**189-192.

Oltvai, Z. N., Milliman, C. L., Korsmeyer, S. J. 1993. Bcl-2 heterodimerizes *in vivo* with a conserved homologue, Bax, that accelerates programmed cell death. *Cell* **74:**609-619.

Oppenheim, R. W. 1991. Cell death during development of the nervous system. *Ann. Rev. Neurosci.* **14:**453-501.

Porter, A.G., Ng, P., Janicke, R. U. 1997. Death substrates come alive. *Bioessays.* **19:** 501-507.

Pellizzoni, L., Kataoka, N., Charroux, B., Dreyfuss, G. 1998. A novel function for SMN, the spinal muscular atrophy disease gene product, in pre-mRNA splicing. *Cell* **95:**615-624.

Peress, N. S., Stermann, A. B., Miller, R., Kaplan, C. G., Little, B.W. 1986. "Chromalytic" neurons in lateral geniculate body in Werdnig-Hoffmann disease. *Clin Neuropathol.* **5:**69-72.

Raff, M. C., Barres, B. A., Burne, J. F., Coles, H. S., Ishizaki, Y., Jacobson, M. D. 1993. Programmed cell death and the control of cell survival: lessons from the central nervous system. *Science* **262:**467-471.

Reed, J.C. 1999. Dysregulation of apoptosis in cancer. *Journal of Clinical Oncology.* **17:** 2941-2953.

Rodrigues, N. R., Owen, N., Talbot, K., Ignatius, J., Dubowitz, V., Davies, K. E. (1995). Deletions in the survival motor neuron gene on 5q13 in autosomal recessive spinal muscular atrophy. *Hum. Mol. Genet.* **4:**631- 634.

Rodrigues, N., Owen, N., Talbot, K., Pate, S., Muntoni, F., Ignatius, J., Dubowitz, V., Davies, K. E. 1996. Gene deletions in spinal muscular atrophy. *J. Med. Gen.* **33:**93-96.

Roy, N., Deveraux, Q. L., Takahashi, R., Salvesen, G .S., Reed, J. C. 1997. The cIAP-1 and cIAP-2 proteins are direct inhibitors of specific caspases. *EMBO J.* **16:**6914-6925.

Roy, N., Mahadevan, M. S., McLean, M., Shutler, G., Yaraghi, Z., Farahani, R., Baird, S., Besner-Johnson, A., Lefebvre, C., Kang, X., Salih, M. Aubry, H., Tamai, K., Ioannou, P., Crawford, T., de Jong, P., Surh, L., Ikeda, J., Korneluk, R., Mackenzie, A. 1995. The gene for neuronal apoptosis inhibitory protein is partially deleted in individuals with spinal muscular atrophy. *Cell* **80:**167-178.

Russman, B. S., Iannacone, S.T., Buncher, C.R., Samaha, F.J., White, M., Perkins, B., Zimmerman, L., Smith, C., Burhans, K., Barker, L. 1992. Spinal muscular atrophy: new thoughts on the pathogenesis and classification schema. *Journal of Childhood Neurology.* **7:**347-353.

Sarnat, H. B. 1984. Commentary: Research strategies in spinal muscular atrophy. In: *Progressive Spinal Muscular Atrophies* (I. Gamstorp and H. B. Sarnat, Eds.), p233. Raven Press, New York.

Sassoon, D., Lyons, G., Wright, W. E., Lin., V., Lassar, A., Weintraub, H., Buckingham, M. 1989. Expression of two myogenic regulatory factors myogenin and MyoD1 during mouse embryogenesis. *Nature* **341:**303-307.

Scharf, J. M., Damron, D., Frisella, A., Bruno, S., Beggs, A., Kunkel, L., Dietrich, W. 1996. The mouse region syntenic for human spinal muscular atrophy lies within the *Lgn1* critical interval and contains multiple copies of *Naip* exon 5. *Genomics* **38:**405-417.

Scharf, J. M., Endrizzi, M. G., Wetter, A., Huang, S., Thompson, T. G., Zerres, K., Dietrich, W. F., Wirh, B., Kunkel, L. 1998. Identification of a candidate modifying gene for spinal muscular atrophy by comparative genomics. *Nature Genet.* **20:**83-86.

Schrank, B., Gotz, R., Gunnersen, J. M., Ure, J. M., Toyka, K., Smith, A., Sendtner, M. 1997. Inactivation of the survival motor neuron gene, a candidate gene for human spinal muscular atrophy, leads to massive cell death in early mouse embryos. *Proc. Natl. Acad. Sci USA* **94:**9920-9925.

Schwartz, L., M., Osborne, B. 1993. Programmed cell death, apoptosis and killer genes. *Immunology today* **14:**582-590.

Shindler, K. S., Latham, C. B., Roth, K. A. 1997. Bax deficiency prevents the increased cell death of immature neurons in the bcl-x deficient mice. *J Neurosci.* **17:**3112-3119.

Shuler, C.F. 1995. Programmed cell death and cell transformation in the craniofacial development. *Crit. Rev. Oral. Biol. Med.* **6:**202-217.

Silva, M., Grillot, D., Benito, A., Nunez, G., Fernadez- Luna, J. L. 1996. Erythropoietin can promote erythroid progenitor survival by repressing apoptosis through Bcl-XL and Bcl-2. *Blood.* **88:**1576-1582.

Sohma, O., Mizuguchi, M., Takashima, S., Yamada, M., Ikeda, K., Ohta,S. 1996. High expression of bcl-x protein in the developing human cerebellar cortex. *J. Neurosci. Res.* **43:** 175-182.

Stefanis, L., Burke, R. E., Greene, L. A. 1997. Apoptosis in neurodegenerative disorders. *Current Opinion in Neurology.* **10:**299-305.

Steiman, G.S., Rorke, L. B., Brown, M.J. 1980. Infantile neuronal degeneration masquerading as Werdnig-Hoffmann disease. *Annals of Neurology.* **8:**317-324.

Strong, T. W., Tagle, D., Valdes, J., Elmer, L., Boehm, K., Swaroop, M., Kaatz, K., Collins, F., Albin, R. 1993. Widespread expression of the human and rat Huntington's disease gene in brain and non-neural tissues. *Nature Genet.* **5:**259-265.

Tizzano, E., Cabot, C., Baiget, M. 1998. Cell- Specific survival motor neuron gene expression during human development of the central nervous system. *Am.J.of Path.* **153:** 355-361.

Towfighi,J., Young, R.S.K., Ward, R. 1985. Is Werding-Hoffmann disease a pure lower motor neuron disease? *Acta Neuropathol.* **65:**270-280.

Traber, P.1994. Differentiation of intestinal epithelial cells: Lessons from the study of intestine-specific gene expression. *J Lab Clin. Med.* **123:**467-477.

Trier, J.S., Moxey, P.C. 1979 Morphogenesis of the small intestine during fetal development. *Ciba Found Symp* **70:** 3-29.

Tsujimoto, Y., Croce, C. M. 1986. Analysis of the structure, transcripts, and protein products of *bcl-2*, the gene involved in human follicular lymphoma. *Proc. Natl. Acad. Sci. USA* **83:**5214- 5218.

Urase, K., Fujita, E., Miho, Y., Kouroko, Y., Mukasa, T., Yagi, Y., Momoi, M., Momoi, T. 1998. Detection of activated Caspase-3 (CPP32) in the vertebrate nervous system during development by cleavage site- directed antiserum. *Developmental Brain Research.***111:** 77-87.

Velasco, E., Valero, C., Valero, A., Moreno, F., Hernandez- Chico, C. 1996. Molecular analysis of the SMN and NAIP genes in Spanish spinal muscular atrophy (SMA) families and correlation between number of cBCD541 and SMA phenotype. *Hum. Mol. Genet.* **5:** 257-263.

Viollet, L., Bertrandy, S., Bueno Brunialti, A., Lefebvre, S., Burlet, P., Clermont, O., Cruaud, C., Guenet, J. Munnich, A., Melki, J. 1997. cDNA isolation , expression and chromosomal localization of the mouse survival motor neuron gene (Smn). *Genomics.* **40:**185-188.

Westcarr, S., Farshori, P., Wyche, J., Anderson, W. 1999. Apoptosis and differentiation in the crypt-villus unit of the rat small intestine. *J Submicrosc Cytol Pathol.* **31:**15-30.

White, F. A., Keller-Peck, C. R., Knudson, C. M. Korsmeyer, S. J., Snider, W. D. 1998. Widespread elimination of naturally occurring neuronal death in Bax- deficient mice. *J Neurosc.* **18:**1428-1439.

Wilkinson, D. G., Bailes, J. A., Champion, J. E., McMahon, A. P. 1987. A molecular analysis of mouse development from 8 to 10 days *post coitum* detects changes only in embryonic globin expression. *Development.* **99:**493-500.

Wilkinson, D. G. (1992) *In Situ* Hybridization: A Practical Approach. In: Wilkinson DG, ed. Oxford: IRL Press at Oxford University Press, 1992.

Wyllie, A. H., Kerr, J. F. R., Currie, A. R., 1980. Cell death: the significance of apoptosis. *Int Rev Cytol.* **68:**251-306.

Wyllie, A. H., Morris, R.G., Smith, A. L., Dunlop, D. 1984. Chromatin cleavage in apoptosis: association with condensed chromatin morphology and dependence on macromolecular synthesis. *J Pathol* **142:**67-77.

Xu, D., Crocker, S. J., Doucet, J.P., St-Jean, M., Tamai, K., Hakim, A. M., Ikeda, J. E., Liston, P., Thompson, C., Korneluk, R. G., MacKenzie, A.E., Robertson, G. S.1997a. Elevation of neuronal expression of NAIP reduces ischemic damage in the hippocampus. *Nature Med* **9:**997-1004.

Xu, D. Korneluk, R. G., Tamai, K., Wigle, N., Hakim, A. M., MacKenzie, A., Robertson, G.S. 1997b. Distribution of neuronal apoptosis inhibitory protein-like immunoreactivity in the rat central nervous system. *J. Comp. Neuro.* **381:**1-13.

Yachnis, A., Giovanini, M., Eskin, T., Reir, P., Anderson, D. 1998. Developmental patterns of BCL-2 and BCL-X polypeptide expression in the human spinal cord. *Exp Neurology.* **150:**82-97.

Yaraghi, Z., Korneluk, G., MacKenzie, A. 1998. Cloning and characterization of the multiple murine homologues of *NAIP* (Neuronal Apoptosis Inhibitory Protein). *Genomics.* **51:**107-113.

Yaraghi, Z., Diez, E., Gros, P., MacKenzie, A. 1999 cDNA cloning and the 5'genomic organization of Naip2, a candidate gene for murine Legionella resistance. *Mamm Genome* **10** 761-763.

Yoshida, H., Kong, Y. Y., Yoshida, R., Elia, A. J., Hakem, A., Hakem, R., Penninger, J. M., Mak, T. W.1998. Apaf-1 is required for mitochondrial pathways of apoptosis and brain development. *Cell* **94:** 739-750.

Young, R.W. 1984. Cell death during differentiation of the retina in the mouse. *J Comp Neurol.* **229:**362-373.

Yuan, J., Horvitz, H. R. 1992. The *C. Elegans* cell death gene *ced-4* encodes a novel protein and is expressed during the period of extensive cell death. *Development* **116:**309-320

Yuan, J., Shaham, S., Ledoux, S., Ellis, h. M., Horvitz, H. R. 1993. The *C. elegans* cell death gene *ced*-3 encodes a protein similar to mammalian interlukin-1β-converting enzyme. *Cell* **75:**641-652.